Helicobacter pylori provokes STING immunosurveillance via trans-kingdom conjugation

Prashant P. Damke[1*], Cecily R. Wood[1*], and Carrie L. Shaffer[1,2,3,4#]

Affiliations

1. Department of Veterinary Sciences, University of Kentucky College of Agriculture, Lexington, KY, 40546, USA
2. Department of Microbiology, Immunology, and Molecular Genetics, University of Kentucky College of Medicine, Lexington, KY, 40506, USA
3. Department of Pharmaceutical Sciences, University of Kentucky College of Pharmacy, Lexington, KY, 40536, USA
4. Markey Cancer Center, University of Kentucky College of Medicine, Lexington, KY, 40506, USA

*These authors contributed equally

[#]Corresponding author: carrie.shaffer@uky.edu

Keywords: *Helicobacter pylori,* type IV secretion system, T4SS, gastric cancer, cGAS, STING, bacterial pathogenesis

ABSTRACT

Recognition of foreign nucleic acids is an evolutionarily conserved mechanism by which the host detects microbial threats. Whereas some intracellular bacterial pathogens trigger DNA surveillance pathways following phagosomal membrane perturbation, mechanisms by which extracellular bacteria activate cytosolic nucleic acid reconnaissance systems remain unresolved. Here, we demonstrate that *Helicobacter pylori* exploits *cag* type IV secretion system (*cag* T4SS) activity to provoke STING signaling in gastric epithelial cells. We provide direct evidence that chromosomal fragments delivered to the host cell cytoplasm via trans-kingdom conjugation bind and activate the key DNA sensor cGMP-AMP synthase. To enable paracrine-like signal amplification, translocated *H. pylori* DNA is sorted into exosomes that stimulate DNA-sensing pathways in uninfected bystander cells. We show that DNA cargo is loaded into the *cag* T4SS apparatus in the absence of host cell contact to establish a 'ready-to-fire' nanomachine and provide evidence that *cag* T4SS-dependent DNA translocation is mechanistically coupled to chromosomal replication and replichore decatenation. Collectively, these studies suggest that *H. pylori* evolved mechanisms to stimulate nucleic acid surveillance pathways that regulate both pro- and anti-inflammatory programs to facilitate chronic persistence in the gastric niche.

INTRODUCTION

Innate recognition of invariant pathogen-associated molecular signatures by cellular pattern recognition receptors (PRRs) is the first line of defense against microbial adversaries. Within the gastrointestinal tract, epithelial cells express proximal endosomal and cytosolic nucleic acid-sensing PRRs that rapidly respond to aberrant microbial DNA and RNA to trigger innate defense mechanisms and coordinate adaptative immunity. Localization of foreign DNA to the host cell cytosol activates multiple nucleic acid reconnaissance systems including the key DNA sensor nucleotidyltransferase cyclic GMP-AMP synthase (cGAS) (Cai et al., 2014; Diner et al., 2013; Sun et al., 2013; Wu et al., 2013). Upon binding DNA originating from either extrinsic or intrinsic sources, cGAS catalyzes the formation of the non-canonical cyclic di-nucleotide 2'3'-cGAMP using ATP and GTP as substrates (Diner et al., 2013; Gao et al., 2013a; Gao et al., 2013b; Sun et al., 2013; Zhang et al., 2013). In turn, 2'3'-cGAMP stimulates the endoplasmic reticulum receptor STING (stimulator of interferon genes) to elicit interferon (IFN) signaling and the production of multifarious inflammatory cytokines (Ishii et al., 2006; Ishikawa and Barber, 2008; Ishikawa et al., 2009; Stetson and Medzhitov, 2006; Sun et al., 2009; Zhong et al., 2008). Dysregulation of mucosal STING signaling can disrupt gut homeostasis and generate pro-tumorigenic inflammatory microenvironments (Ke et al., 2022); however, the outcomes of STING-dependent immune surveillance within the context of gastric inflammation and infection-associated carcinogenesis remain unresolved.

Of the known infection-associated cancers, the most significant carcinogenic microbe is the gastric bacterium *Helicobacter pylori*, which chronically colonizes the stomach of over half of the global population and directly contributes to the development of more than one million new cases of cancer per year (Sung et al., 2021). *H. pylori* harboring the cancer-associated *cag* type IV secretion system (*cag* T4SS) significantly augment disease risk via translocation of pro-inflammatory molecular cargo into gastric epithelial cells. In addition to facilitating the delivery of the bacterial oncoprotein CagA, the *cag* T4SS translocates a diverse repertoire of immunostimulatory lipid, nucleic acid, and polysaccharide substrates directly into the gastric epithelium (Amieva and Peek, 2016; Cover et al., 2020). Recent work reported that *H. pylori cag* T4SS activity activates the endosomal DNA-sensing PRR Toll-like Receptor 9 (TLR9), leading to immune suppression conferring tolerance (Varga et al., 2016a; Varga et al., 2016b) as well as other potential inflammation-independent carcinogenic phenotypes (Castano-Rodriguez et al., 2014). In addition to TLR9, multiple cellular nucleic acid sensors, including cGAS (Ablasser et al., 2013; Cai et al., 2014; Diner et al., 2013; Gao et al., 2015; Nandakumar et al., 2019; Storek et al., 2015; Watson et al., 2015; Zhang et al., 2014), RIG-I (Chow et al., 2015; Dixit and Kagan, 2013; Onomoto et al., 2021; Rad et al., 2009), MDA5 (Dixit and Kagan, 2013; Wu et al., 2020), AIM2 (Rathinam et al., 2010), ZBP1/DAI (Kuriakose et al., 2016), IFI-16 (Almine et al., 2017; Unterholzner et al., 2010), and RNA pol III (Ablasser et al., 2009; Chiu et al., 2009) are expressed in the human gastric epithelium and associated mucosal dendritic cells (Rad et al., 2009), raising the hypothesis that *H. pylori* stimulates additional innate nucleic acid surveillance pathways.

While intracellular bacterial pathogens elicit cGAS-STING signaling following phagosomal membrane destabilization or rupture achieved in a type III, IV, VI, or VII secretion system-dependent manner (Ku et al., 2020; Marinho et al., 2017; Nandakumar et al., 2019; Storek et al., 2015; Watson et al., 2015; Zhang et al., 2014), the mechanisms by which extracellular bacteria stimulate DNA reconnaissance systems remain unclear. STING signaling has been implicated in gastric carcinogenesis and *H. pylori* has been shown to activate STING *in vivo* (Song et al., 2017), but whether *H. pylori*-driven STING activation requires cytosolic nucleic acid immunosurvellience is unknown. Here, we demonstrate that *H. pylori*-induced STING signaling is a direct consequence of *cag* T4SS-dependent DNA translocation. We show that *H. pylori* chromosomal fragments delivered to the gastric epithelium via trans-kingdom conjugation directly bind and

activate cGAS to stimulate STING signaling. We discovered that upon translocation into primary gastric epithelial cells, fragmented *H. pylori* DNA is sorted into exosomes that are released to amplify foreign nucleic acid immune surveillance in uninfected bystander cells. We provide direct evidence that *cag* T4SS-mediated DNA translocation is mechanistically coupled to chromosomal replication and demonstrate that eukaryotic-optimized constructs greater than 1.5 kb are delivered to the gastric epithelium via *cag* T4SS mechanisms. Our results highlight how *H. pylori* exploits the versatile *cag* T4SS to tip the delicate STING signaling balance towards inflammatory responses that may stimulate carcinogenesis and enable chronic colonization of the gastric niche.

RESULTS

***H. pylori* provokes multiple DNA surveillance systems in a *cag* T4SS-dependent manner.** Previous studies demonstrate the capacity of *H. pylori* to stimulate DNA-sensing pattern recognition receptors, including TLR9 (Rad et al., 2009; Varga et al., 2016b), raising the hypothesis that microbial nucleic acids are actively translocated into host cells. In agreement with previous reports (Rad et al., 2009; Varga et al., 2016b), *H. pylori* challenge of HEK293 reporter cell lines stably transfected with TLR9 demonstrated that *cag* T4SS activity is required for TLR9 stimulation (**Fig. 1A,B**). Consistent with the observation that CagA is not translocated into HEK293 cells (Kumar Pachathundikandi et al., 2011; Varga et al., 2016b), disruption of *cagA* did not diminish levels of *H. pylori*-induced TLR9 activation (**Fig. 1A and Fig. S1A**). To confirm that a functional *cag* T4SS is required to activate TLR9, we co-cultured TLR9 reporter cells with a *cagL* isogenic mutant or the corresponding genetically complemented strain. Whereas inactivation of *cagL* abrogated TLR9 activation, complementation in a heterologous chromosomal locus rescued TLR9 stimulation to levels indistinguishable from the parental WT strain (**Fig. 1B**). In concert with previous investigations, these data demonstrate that *cag* T4SS activity, but not CagA delivery, is required for robust TLR9 signaling.

In addition to endosomal DNA pattern recognition receptors such as TLR9, gastric epithelial cells harbor cytosolic DNA surveillance proteins including the nucleotidyltransferase cyclic GMP-AMP (cGAMP) synthase (Cai et al., 2014; Diner et al., 2013; Sun et al., 2013; Wu et al., 2013). To test whether *H. pylori* DNA is trafficked into the host cell cytoplasm to activate cytosolic DNA surveillance sensors, we challenged 293T cells transfected with constructs to enable cGAS and STING expression and quantified levels of IFN-β promoter-driven luciferase produced in response to *H. pylori*. Compared to mock infected cells, WT *H. pylori* stimulated high levels of cGAS-STING signaling at 18 h post-infection. Similar to TLR9 activation assays, the *cagL* mutant was unable to stimulate robust cGAS-STING signaling, a phenotype that was restored by genetic complementation in a secondary chromosomal locus (**Fig. 1C**). In contrast to HEK293-hTLR9 cells, moderate levels of translocated CagA were detected in 293T cells co-cultured with WT *H. pylori* but not in corresponding *cagE*-challenged monolayers (**Fig. S1A**). Although *H. pylori* has the capacity to deliver CagA into 293T cells, disruption of *cagA* did not significantly alter levels of *cag* T4SS-dependent IFN-β promoter activity in cGAS-STING reporter cells (**Fig. S1B**). To exclude the possibility that cGAS-STING activation results from bacterial endocytosis or increased bacterial interaction with host cell surfaces, we performed gentamicin protection assays. In contrast to marked differences in cGAS-STING activation elicited by WT and *cagX,* equivalent levels of adherent and intracellular bacteria were recovered from 293T co-cultures, confirming that cGAS-STING signaling is not an artifact of non-specific bacterial internalization or spontaneous bacterial lysis (**Fig. S1C**).

Previous studies demonstrate that in addition to detecting invading microbial threats, cGAS senses and responds to DNA damage and genomic instability (Cai et al., 2014; Ke et al., 2022). *H. pylori cag* T4SS activity is directly linked to nuclear double-stranded DNA (dsDNA) breaks introduced in response to ALPK1/TIFA signaling stimulated by D-glycero-beta-D-manno-heptose

143 1,7-bisphosphate (HBP) or ADP-beta-D-manno-heptose (β-ADP-heptose) translocation (Bauer et
144 al., 2020; Gall et al., 2017; Zimmermann et al., 2017). We therefore addressed the possibility that
145 *cag* T4SS-dependent nuclear DNA damage stimulates cGAS-STING signaling elicited by WT *H.*
146 *pylori*. Disruption of *rfaE*, the enzyme responsible for β-ADP-heptose production (Bauer et al.,
147 2020; Gall et al., 2017; Stein et al., 2017; Zimmermann et al., 2017), did not impact the level of
148 cGAS-STING signaling achieved by *H. pylori* (**Fig. 1D**), indicating that ALPK1/TIFA signaling-
149 induced DNA damage does not significantly contribute to *H. pylori*-driven cGAS activation *in vitro*.
150 In addition to ALPK1/TIFA-mediated DNA modifications (Bauer et al., 2020; Gall et al., 2017; Stein
151 et al., 2017; Zimmermann et al., 2017), *H. pylori* has the capacity to induce production of DNA-
152 damaging reactive oxygen species (ROS) by triggering NF-κB activation and additional
153 mechanisms involving inducible nitric oxide synthase (iNOS) and associated inflammatory
154 enzymes (Bauer et al., 2020; Kidane, 2018). In support of the observation that *cag* T4SS-induced
155 dsDNA breaks are not a significant cGAS activating factor in the context of *H. pylori* infection,
156 cGAS-STING activation was achieved by *H. pylori* co-cultured in the presence of the antioxidant
157 N-acetyl-cysteine at concentrations that abrogate ROS production (Bauer et al., 2020) (**Fig. S1D**).
158
159 Following infection, damaged mitochondria release DNA (mtDNA) and other constituents into the
160 cytosol to act as potent danger-associated molecular patterns (DAMPs) that engage TLR9
161 (Garcia-Martinez et al., 2016; Oka et al., 2012; Zhang et al., 2010) and cGAS-STING signaling
162 axes to initiate type I IFN production (Rongvaux et al., 2014; West et al., 2015; White et al., 2014).
163 To test the hypothesis that *H. pylori cag* T4SS activity modulates mitochondrial integrity resulting
164 in the release of mtDNA and activation of cytosolic DNA-sensing PRRs, we assayed cGAS-
165 STING activation in the presence of BAX/BAK macropore inhibitory peptides that prevent
166 permeabilization of the mitochondrial outer membrane and herniation of mtDNA into the cytosol
167 (McArthur et al., 2018; White et al., 2014). *H. pylori* induced similar levels of cGAS-STING
168 activation in the presence of BAX inhibitory peptide or non-inhibitory peptide control co-cultures
169 (**Fig. S1E**) suggesting that ruptured mitochondria are not the primary source of cGAS-activating
170 DNA. Likewise, treatment of co-cultures with a mitochondria-targeted antioxidant did not
171 significantly alter levels of cGAS-STING signaling (**Fig. S1D**), demonstrating that *H. pylori*-
172 induced mtDNA damage is not a predominant DAMP within the context of *cag* T4SS-dependent
173 cGAS activation. To exclude the possibility that cGAS-STING activation is dependent upon the
174 import of released *H. pylori* DNA via host cell mechanisms, we quantified IFN-β promoter activity
175 produced by cGAS-STING reporter cells that were physically separated from *H. pylori*. In support
176 of the hypothesis that cGAS-STING activation requires direct *H. pylori*-host cell interaction, cGAS
177 stimulation was achieved by *H. pylori* that were in direct contact with reporter cells, but not in
178 samples in which *H. pylori* and reporter cells were physically separated by a 0.4 μM-pore
179 polycarbonate insert (**Fig. 1E**). Collectively, these studies demonstrate that cGAS stimulation is
180 a consequence of *cag* T4SS-dependent DNA delivery into the host cell cytosol.
181
182 To define the role of cGAS in *H. pylori*-driven IFN-β signaling, we next determined whether *cag*
183 T4SS activity could transactivate STING through direct cGAMP transfer via gap junction-mediated
184 diffusion. To assess cGAS signaling *in trans*, 293T cells transfected with cGAS constructs were
185 co-cultured with 293T cells harboring STING and IFN-β reporter constructs, and co-cultures were
186 challenged by *H. pylori* for 18 h. High levels of STING signaling were observed in cells challenged
187 by WT *H. pylori*, but not a *cagX* mutant, suggesting that *cag* T4SS-dependent cGAS stimulation
188 generates sufficient cGAMP for migration into bystander cells (**Fig. 1F**). To examine the
189 requirement of cGAS protein domains in *H. pylori*-induced STING signaling, we next monitored
190 IFN-β activation in 293T cells transfected with constructs to express either cGAS alone or cGAS
191 variants in combination with STING. In comparison to cells transfected with only $cGAS_{WT}$, WT *H.*
192 *pylori* stimulated high levels of IFN-β transcription when $cGAS_{WT}$ and STING were co-expressed

(**Fig. 1G**). In contrast, *cag* T4SS-dependent IFN-β transcription was markedly reduced in 293T cells transfected with STING and cGAS variants lacking the DNA-binding domain ($cGAS_{\Delta DBD}$) or harboring point mutations within nucleotidyltransferase catalytic residues that abolish cGAMP production ($cGAS_{\Delta NTase}$) (**Fig. 1G**). Collectively, these results demonstrate that cGAS senses and responds to *cag* T4SS activity.

A previous report suggests that decreased STING signaling is associated with adverse outcomes in gastric cancer patients (Song et al., 2017). We therefore monitored cGAS-STING signaling induced by several *H. pylori* clinical isolates obtained from patients with gastric diseases of varying severity. In contrast to strains isolated from patients exhibiting gastritis, *H. pylori* isolated from individuals with duodenal ulcers or gastric cancer elicited lower levels of cGAS-STING signaling (**Fig. 1H**), suggesting that *H. pylori* may modulate the capacity to induce *cag* T4SS-dependent STING activation during chronic stomach colonization.

Microbial DNA is delivered to the gastric epithelial cell cytoplasm via *cag* T4SS activity. We next assessed the consequence of *H. pylori* trans-kingdom DNA conjugation within the context of biologically-relevant interactions with gastric epithelial cells. To monitor DNA injection into gastric epithelial cells, AGS cells were challenged by either WT or the *cagX* isogenic mutant at a MOI of 50. After 6 h, gastric epithelial cell co-cultures were treated with DNaseI to remove extracellular DNA and eukaryotic cells were fractionated using digitonin to selectively permeabilize the plasma membrane, leaving the nuclear envelope and bacterial cells intact. PCR analysis of fractionated infected AGS cells revealed the presence of *H. pylori* DNA in cytoplasmic fractions (**Fig. 2A**) with significantly more bacterial DNA present in cytosolic fractions obtained from WT-challenged cells. When comparing the ratio of cytoplasmic bacterial DNA to cytoplasmic-localized mitochondrial DNA by qPCR, significantly more bacterial DNA was present in the cytosol of gastric epithelial cells infected by the WT strain compared to corresponding cells infected by the *cagX* mutant (**Fig. 2B**). Levels of mitochondrial DNA did not significantly differ in cytosolic extracts obtained from infected and uninfected cells (**Fig. 2A**). To exclude the possibility that cytosolic localization of *H. pylori* DNA resulted from non-specific bacterial lysis or endocytosis, we performed studies to analyze the level of adherent and internalized *H. pylori* in infected gastric epithelial cells. Using gentamicin-protection assays, we determined that similar levels of adherent and intracellular WT and *cagX* bacteria were recovered from AGS co-cultures (data not shown). Multiple cancer cell lines, including cell lines derived from gastric adenocarcinoma, continuously export low levels of extracellular cGAMP that serves as a potent immunotransmitter (Carozza et al., 2020). We thus measured levels of extracellular cGAMP secreted by AGS cells in response to *H. pylori* challenge. Consistent with the hypothesis that *cag* T4SS-mediated DNA delivery stimulates cytosolic cGAS and the subsequent production of cGAMP, the level of extracellular cGAMP was significantly higher in supernatants obtained from WT-challenged co-cultures compared to mock infected or corresponding *cagX*-challenged monolayers (**Fig. 2C**). Collectively, these results suggest that the presence of bacterial DNA in the host cell cytoplasm is a consequence of *cag* T4SS activity and leads to the production of cGAS-generated cGAMP.

Although gastric adenocarcinoma cell lines (including AGS and MKN45) produce detectable levels of cGAS and other nucleic acid-sensing PRRs, STING expression is absent (Qiao et al., 2020). To determine whether translocated *H. pylori* DNA elicits cGAS-STING responses in normal gastric epithelia, we challenged primary adult gastric epithelial cells with *H. pylori* and monitored the formation of peri-nuclear STING polymers that aggregate in response to cGAMP binding. Compared to mock infected or *cagX*-challenged cells, WT *H. pylori* induced the formation of large STING aggregates that could be visualized by confocal microscopy (**Fig. 2D**). Consistent with activation of cGAS-STING signaling, quantification of the average STING polymer size in *H. pylori*-gastric cell co-cultures revealed significantly larger STING aggregates in WT-challenged

244 cells (**Fig. 2E**), suggesting *cag* T4SS-dependent stimulation of cGAS surveillance. In addition to
245 cGAS, epithelial cells harbor other nucleic acid reconnaissance systems that signal through
246 STING. To determine whether *H. pylori* stimulates additional STING-dependent signaling
247 pathways, we analyzed IFN-β activity in 293T-STING cells. Compared to control 293T cells
248 harboring empty vector, *H. pylori* stimulated STING signaling in a *cag* T4SS-dependent manner
249 (**Fig. 2F**). STING signaling was also elicited by transfection of purified, fragmented *H. pylori*
250 chromosomal DNA into IFN-β reporter cells (**Fig. 2F**), suggesting that endogenous 293T cytosolic
251 DNA-sensing pathways respond to *H. pylori* DNA. Together, these studies demonstrate that *H.*
252 *pylori* delivers chromosomal DNA fragments to gastric epithelial cells via *cag* T4SS mechanisms
253 and reveal that endogenous STING-dependent nucleic acid surveillance systems are activated
254 by translocated *H. pylori* DNA.
255
256 **DNA is a specific *cag* T4SS nucleic acid substrate.** We reasoned that in addition to DNA
257 substrates, the *cag* T4SS may translocate RNA or DNA:RNA hybrids into gastric cells to stimulate
258 STING-dependent signaling. Thus, we sought to characterize the innate inflammatory signature
259 elicited by *H. pylori*. Primary adult gastric epithelial cells were mock infected or challenged by
260 either WT or the corresponding *cagX* isogenic mutant prior to isolation of total RNA. To
261 characterize epithelial innate inflammatory responses, gene expression patterns were analyzed
262 at 6 h post-infection using the NanoString Host Response Panel. Compared to mock infected and
263 *cagX*-challenged primary gastric epithelial cell co-cultures, *cag* T4SS activity induced a significant
264 increase in transcripts associated with anti-microbial defense pathways and interferon signaling
265 (**Fig. 3A and Fig. S2**). Hierarchical clustering performed on genes that were differentially
266 expressed in response to *H. pylori* challenge revealed distinct clustering of mock infected and
267 *cagX*-infected co-cultures in comparison to WT challenge (**Fig. S2C**). Comparison of transcripts
268 differentially produced in response to WT versus *cagX H. pylori* identified 134 genes that were
269 upregulated via *cag* T4SS activity, including genes encoding pro-inflammatory chemokines and
270 cytokines (*e.g.*, *CXCL10*, *CXCL8/IL-8*, *TNF*, *IL1B*, *CCL5*), IFN-α/β signaling (*e.g.*, *ISG15*, *IRF1*,
271 *IFI35*, *STAT1*, *IFNAR2, SAMHD1*), and IFN-γ immunoregulatory programs (*e.g.*, *IFNGR2*, *TRIM5*,
272 *GBP4, VCAM1*) (**Fig. 3A,B**). Consistent with the observed gene expression patterns, pathway
273 analysis of genes induced by *cag* T4SS activity demonstrated a significant enrichment in
274 transcripts associated with interferon-regulated nucleic acid reconnaissance programs (**Fig. 3C**).
275 In addition to *cag* T4SS-dependent regulation of the DNA sensor ZBP1, we observed significantly
276 increased transcript levels of several cytosolic RNA-sensing surveillance systems including
277 *DDX58/RIG-I*, RIG-I-like Receptor *IFIH1/MDA5* (Chow et al., 2015; Dixit and Kagan, 2013), and
278 2′-5′-oligoadenylate synthetases *OAS1* and *OAS2* (Schwartz et al., 2020) in WT-infected primary
279 gastric epithelial cells (**Fig. 3A,B**).
280
281 A previous study reported the capacity of gastric mucosa-associated dendritic cells to sense and
282 respond to purified *H. pylori* RNA through RIG-I and TLR7/8, leading to the production of type I
283 IFN (Rad et al., 2009; Salama et al., 2013). However, whether the *cag* T4SS actively translocates
284 RNA to stimulate TLR7/8 or RIG-I signaling axes has not been elucidated. We thus sought to
285 determine whether DNA is a specific *cag* T4SS nucleic acid effector. Challenge of HEK293
286 reporter cell lines expressing either TLR7 (**Fig. 3D**) or RIG-1 (**Fig. 3E**) revealed that in contrast to
287 robust activation of DNA-sensing PRRs, *H. pylori* was unable to activate either endosomal ssRNA
288 (TLR7) or cytoplasmic ssRNA/dsRNA (RIG-I) sensors. Collectively, these data suggest that
289 chromosomally-derived DNA is a specific *cag* T4SS substrate, and provide further evidence that
290 *cag* T4SS-dependent DNA translocation stimulates STING-dependent signaling.
291
292 ***H. pylori cag* T4SS activity stimulates DNA immunosurveillance in bystander cells.** Prior
293 work demonstrates that foreign intracellular bacterial DNA can be delivered to adjacent cells via

294 extracellular vesicles as a mechanism to amplify IFN signaling (Nandakumar et al., 2019). We
295 therefore investigated whether translocated *H. pylori* DNA could be sorted into extracellular
296 vesicles to enable paracrine-like DNA signaling by primary gastric epithelial cells. To test the
297 hypothesis that infected gastric epithelial cells release extracellular vesicles containing *H. pylori*
298 DNA, cell-free supernatants collected from infected primary gastric epithelial donor cells were
299 used to challenge recipient TLR9 reporter cells. Compared to supernatants obtained from either
300 mock infected or *cagX*-challenged co-cultures, supernatants harvested from WT-challenged
301 gastric cells robustly activated TLR9 signaling (**Fig. 4A**). The capacity of infected cell
302 supernatants to activate TLR9 was time dependent, as levels of TLR9 activation increased when
303 reporter cells were treated with supernatants obtained from gastric epithelial cells co-cultured with
304 *H. pylori* for 12 h compared to 6 h (**Fig. 4A**). To exclude the possibility that TLR9 activation
305 resulted from contaminate DNA arising from cell lysis, we quantified the level of cell-free DNA in
306 donor supernatants. TLR9 activation elicited by gastric cell supernatants was not correlated to
307 the level of donor supernatant cell-free DNA (**Fig. 4B**), suggesting that the TLR9-stimulating
308 agonist was enclosed within a host cell-derived delivery mechanism.
309
310 To confirm the role of translocated DNA in transferrable nucleic acid immunosurveillance in
311 bystander cells, donor gastric cell supernatants were treated with DNase alone or in combination
312 with heat prior to co-culture with TLR9 reporter cells. Whereas DNase treatment had a negligible
313 effect on TLR9 stimulating capacity, heat treatment modesty reduced TLR9 responses, which
314 were further reduced when donor supernatants were treated with both heat and DNase prior to
315 reporter cell challenge (**Fig. 4C**). These observations led to the hypothesis that translocated
316 microbial DNA packaged within gastric cell-derived extracellular vesicles, such as exosomes,
317 stimulates nucleic acid reconnaissance systems in bystander cells. To test whether exosome
318 biogenesis is required for the delivery of translocated DNA to uninfected cells, we challenged
319 recipient TLR9 reporter cells with donor supernatants obtained from infected primary gastric
320 epithelial cells cultured in the presence or absence of a neutral sphingomyelinase (nSmase2)
321 inhibitor that prevents exosome release. Compared to untreated and mock infected cells,
322 nSmase2 inhibition led to a significant reduction in TLR9 activation levels elicited by WT-
323 challenged donor cell supernatants (**Fig. 4D**), supporting a role of exosomes in stimulating DNA-
324 sensing pathways in bystander cells. To further investigate whether translocated *H. pylori* DNA
325 was packaged within exosomes released from infected gastric epithelial cells, we isolated CD9,
326 CD63, and CD81-positive exosomes from cell culture supernatants via immunopurification.
327 Analysis by qPCR revealed that exosomes purified from WT-challenged gastric cell supernatants
328 were significantly enriched in *H. pylori* DNA compared to corresponding exosomes obtained from
329 *cagX*-challenged co-cultures (**Fig. 4E**), suggesting that foreign bacterial DNA is sorted into
330 exosomes for paracrine-like DAMP signal amplification (**Fig. 4F**).
331
332 **Random chromosomal fragments are delivered to target cells via *cag* T4SS-dependent**
333 **mechanisms.** To identify whether a specific DNA sequence is excised and transferred to host
334 cells by *cag* T4SS activity, we purified cGAS-DNA complexes using modified ChIP-seq workflows
335 to capture bacterial DNA that physically binds and activates cGAS. 293T-cGAS cells were
336 challenged by *H. pylori* for 6 h, followed by chemical cross-linking and immunopurification of
337 cGAS. Deep sequencing analysis confirmed that co-purifying *H. pylori* DNA isolated from WT and
338 *cagX*-infected cells mapped across the entire *H. pylori* chromosome, with significantly more
339 bacterial DNA reads associated with cGAS purifications obtained from WT-challenged
340 monolayers (**Fig. 5A**). Normalized sequencing reads and differential peak calling approaches
341 identified more than three hundred *H. pylori* chromosomal regions specifically associated with
342 cGAS purified from WT-infected cells compared to eight bacterial DNA peaks associated with
343 corresponding preparations obtained from *cagX* co-cultures (P=0.01). When enriched peak
344 centers were mapped to the coordinate position across the *H. pylori* chromosome, differentially

345 enriched peaks heavily clustered around the *oriC* region, with few peaks mapping to the
346 chromosomal region diametrically opposed to *oriC* (**Fig. 5B**), suggesting that DNA translocation
347 is linked to bi-directional DNA replication.
348
349 To test the hypothesis that chromosomal regions near *oriC* are translocated to gastric epithelial
350 cells at a high frequency, we cloned a CMV promoter-driven monomeric nanoluciferase construct
351 into the *ureA* locus (*hp0073*) adjacent to *oriC* (**Fig. 5C**). Gastric epithelial cells and 293T cells
352 were challenged by WT or *cagX H. pylori* strains harboring the eukaryotic-optimized
353 nanolucifersase expression construct (WT_{NL} and $cagX_{NL}$, respectively), and luciferase activity in
354 infected cell lysates was monitored by bioluminescence. Compared to mock infected and $cagX_{NL}$-
355 infected cells, AGS and 293T cells challenged by WT_{NL} produced high levels of bioluminescence
356 (**Fig. 5D** and **5E**), indicating that nanoluciferase production by epithelial cells is linked to *cag*
357 T4SS-dependent DNA translocation.
358
359 To confirm that targeted DNA fragments proximal to *oriC* can be transferred to host cells via cag
360 T4SS mechanisms, we replaced the nanoluciferase gene with a eukaryotic-optimized construct
361 designed to express monomeric mScarlet tethered to the LifeAct N-terminal peptide to enable live
362 cell visualization of F-actin. Microscopy analysis of AGS (**Fig. 5F**) and 293T (**Fig. 5G**) monolayers
363 challenged by $WT_{mScarlet}$ revealed numerous mScarlet-positive cells compared to corresponding
364 $cagX_{mScarlet}$-infected co-cultures. Flow cytometry analysis confirmed our observation that
365 significantly more mScarlet-positive epithelial cells were generated when monolayers were
366 challenged by $WT_{mScarlet}$ compared to T4SS-deficient controls (**Fig. 5H-K**). Together, these data
367 provide direct evidence that targeted chromosomal fragments greater than 1.5 kb in length are
368 excised and delivered to host cells via *cag* T4SS-dependent mechanisms.
369
370 ***H. pylori* trans-kingdom conjugation is mechanistically coupled to chromosomal**
371 **decatenation.** We next sought to understand the mechanism by which effector DNA is coupled
372 to the *cag* T4SS for transfer to target host cells. The observation that fragments of translocated
373 bacterial DNA map predominantly to the *oriC* region led to the hypothesis that *H. pylori* trans-
374 kingdom conjugation is linked to chromosomal replication. In support of this hypothesis, *cag*
375 T4SS-dependent TLR9 activation was significantly impaired in the presence of the DNA gyrase
376 inhibitor ciprofloxacin in a dose-dependent manner (**Fig. 6A**). To analyze the contribution of DNA
377 segregation proteins to coupling transfer DNA to the *cag* T4SS apparatus, we employed targeted
378 mutagenesis to delete individual genes known to be involved in DNA partitioning. Whereas
379 isogeneic mutants deficient in genes encoding the DNA partitioning proteins ParA or ParB
380 induced WT levels of *cag* T4SS-depenedent TLR9 activation, isogenic mutants lacking genes
381 encoding the DNA translocase *ftsK* (*hp1090*) or the recombinase *xerH* (*hp0675*) exhibited marked
382 defects in TLR9 stimulation (**Fig. 6B**), suggesting that chromosomal dimer resolution is required
383 for transfer DNA coupling to the *cag* T4SS apparatus. TLR9 stimulation defects exhibited by the
384 *ftsK* mutant could be rescued by genetic complementation with full length FtsK, but not a truncated
385 FtsK harboring only the translocase DNA binding domain (FtsK-γ), which is required for interaction
386 with XerH and XerH-mediated DNA recombination (Debowski et al., 2012) (**Fig. 6B**). Loss of *xerH*
387 or *ftsK* was not associated with defects in *cag* T4SS-dependent induction of IL-8 synthesis by
388 gastric epithelial cells (**Fig. 6C**), indicating that chromosomal segregation defects specifically
389 impair *cag* T4SS phenotypes associated with DNA translocation. Consistent with the observed
390 defects in TLR9 activation, *ftsK* mutants stimulated significantly reduced levels of cGAS-STING
391 signaling compared to WT and the corresponding FtsK complemented strain (**Fig. 6D**).
392
393 To investigate the role of chromosomal segregation in loading effector DNA into the *cag* T4SS
394 apparatus, we developed a 'transfer DNA' immunopurification assay to capture chromosomal
395 fragments contained within the *cag* T4SS translocation channel. We reasoned that effector DNA

396 trafficked into the *cag* T4SS apparatus would physically interact with components of the outer
397 membrane complex that comprise the secretion chamber (Chung et al., 2019; Frick-Cheng et al.,
398 2016). To test this hypothesis, we treated *H. pylori* with formaldehyde to chemically cross-link
399 DNA-protein complexes, lysed the cells by sonication, and purified the *cag* T4SS core complex
400 via immunopurification targeting CagY, which forms the central cap-like structure within the inner
401 ring of the outer membrane complex (Chung et al., 2019). PCR analysis targeting a 795 bp
402 chromosomal fragment revealed the presence of DNA in reverse cross-linked CagY complexes
403 purified from WT but not in mock preparations obtained from *cagY* isogenic mutants (**Fig. 6E**).
404 DNA co-purification with CagY was not dependent on the presence of either the effector protein
405 CagA or CagT, a component localized to the periphery of the outer membrane ring complex
406 (Chung et al., 2019; Frick-Cheng et al., 2016); however, DNA loading into the *cag* T4SS apparatus
407 was significantly impaired in the absence of FtsK (**Fig. 6E**). Together, these data demonstrate
408 that effector DNA is loaded into the *cag* T4SS machinery prior to encountering host cells to
409 establish a 'ready-to-fire' nanomachine and demonstrate that transfer DNA loading is
410 mechanistically coupled to chromosomal replication and replichore decatenation. We thus
411 propose a model in which FtsK-XerH complexes resolve imbalanced replichores arising from
412 overlapping rounds of chromosomal replication, resulting in the rare excision of DNA that is
413 subsequently shuttled through the *cag* T4SS apparatus via unknown mechanisms (**Fig. 6F**).
414
415 **DISCUSSION**
416 STING-dependent immunosurveillance plays a critical role in maintaining gastric mucosal
417 homeostasis and regulating inflammatory responses with carcinogenic potential (Ke et al., 2022).
418 STING signaling has been implicated in the development and progression of stomach cancer, but
419 whether STING activation promotes or restricts gastric carcinogenesis remains unresolved. For
420 example, a previous study demonstrated that STING downregulation in primary gastric tumors
421 was associated with increased malignancy and the progression of gastric cancer (Song et al.,
422 2017), while a conflicting report determined that high STING expression in malignant tissues and
423 tumor-associated macrophages was predictive of poor prognosis in stomach cancer patients
424 (Miao et al., 2020). Thus, the molecular role of cGAS-STING signaling in chronic gastric
425 inflammation and pre-malignant lesion development remains unresolved. Consistent with the
426 observation that chronic *H. pylori* colonization elicits STING signaling in the murine gastric
427 mucosa (Song et al., 2017), our study establishes a critical role of *cag* T4SS-mediated trans-
428 kingdom DNA conjugation in stimulating STING-dependent outcomes that underscore infection-
429 associated carcinogenesis.
430
431 In the context of bacterial infection, type I IFN responses have been associated with both
432 protective and detrimental outcomes (Boxx and Cheng, 2016; Peignier and Parker, 2021).
433 Previous work demonstrates that the *H. pylori cag* T4SS-dependent delivery of muropeptide
434 fragments activates Nod1 sensing and IRF7-mediated type I IFN responses in epithelial cells that
435 restrict bacterial proliferation via CXCL10-mediated immune cell recruitment (Viala et al., 2004;
436 Watanabe et al., 2010). Our work demonstrates that during acute infection, CXCL10 is highly
437 upregulated by *cag* T4SS activity in primary gastric epithelial cells (**Fig. 3**). In addition to increased
438 transcript levels associated with interferon stimulated genes, we observed augmented production
439 of transcripts associated with *SMHD1* [a suppressor of type I IFN and NF-κB signaling (Chen et
440 al., 2018)], *IFI35* [a negative regulator of RIG-I signaling (Das et al., 2014)], and *ISG15* [an IFN-
441 α/β-inducible ubiquitin-like modifier that is a key negative regulator of IFN-α/β immunity (Zhang et
442 al., 2015)] in WT-infected primary gastric cells, suggesting that *H. pylori* has evolved mechanisms
443 to counteract or suppress nucleic acid signaling pathways induced by *cag* T4SS activity. We
444 speculate that similar to evasion strategies employed by numerous viruses, *H. pylori* counteracts
445 type I IFN responses through the *cag* T4SS-dependent translocation of as yet unidentified,
446 evolutionarily-conserved protein effectors that target and neutralize components of DNA-sensing

447 or STING signaling pathways. Alternatively, pro-inflammatory STING signaling may balance
448 immunosuppressive responses stimulated by *cag* T4SS-dependent TLR9 activation (Varga et al.,
449 2016a) as a mechanism to sustain gastric homeostasis during acute colonization.
450
451 Epithelial DNA damage, genomic alterations, and chromosomal instability are hallmarks of *H.*
452 *pylori*-induced gastric cancer (Chaturvedi et al., 2014). While *H. pylori cag* T4SS activity has been
453 shown to induce the formation of both double-stranded DNA breaks (DSBs) and micronuclei that
454 potentially contribute to cGAS-STING signaling in gastric epithelial cells (Bauer et al., 2020;
455 Hanada et al., 2014; Koeppel et al., 2015), our data suggest that translocated chromosomal DNA
456 fragments serve as the predominant cytosolic cGAS trigger in the context of *H. pylori* infection
457 (**Fig. 1** and **Fig. S1**). In support of our data indicating that translocated chromosomal fragments
458 are the key agonist that alerts cytosolic nucleic acid surveillance, we found that *H. pylori* effector
459 DNA is packaged into exosomes released by gastric epithelial cells to enable paracrine-like signal
460 amplification (**Fig. 4**). Consistent with a previous study demonstrating that intracellular *Listeria*
461 *monocytogenes* infection stimulates the production of extracellular vesicles with IFN-inducing
462 potential (Nandakumar et al., 2019), the delivery of pathogen-derived DNA via exosome release
463 may represent a conserved mechanism by which epithelial cells potentiate nucleic acid
464 surveillance-dependent danger signaling to uninfected tissues. We propose that *H. pylori* has
465 evolved to exploit this innate defense mechanism to shape a tolerogenic immune response that
466 favors persistent gastric colonization (Varga et al., 2016a).
467
468 Mechanistically, our data demonstrate that *cag* T4SS-dependent DNA delivery is coupled to
469 chromosomal replication and replichore decatenation (**Fig. 5** and **Fig. 6**). Similar to *Neisseria*
470 *gonorrhoeae* ssDNA secretion mechanisms (Callaghan et al., 2017), chromosomal partitioning
471 influences *cag* T4SS-mediated DNA translocation. Indeed, our studies reveal that effector DNA
472 coupling to the *cag* T4SS apparatus requires both FtsK membrane tethering and DNA translocase
473 activity (**Fig. 6**). In support of the critical role of replichore decatenation in *cag* T4SS-dependent
474 DNA translocation, *H. pylori* lacking the DNA recombinase XerH, which requires direct interaction
475 with FtsK to resolve chromosome dimers and catenated chromosomes (Bebel et al., 2016;
476 Debowski et al., 2012), exhibited significantly reduced levels of TLR9 stimulation. Our studies
477 suggest that while *xerH* mutants harbor increased DNA content per cell compared to the parental
478 WT strain (Debowski et al., 2012), *cag* T4SS DNA translocation phenotypes are significantly
479 impaired when chromosomal DNA topological isomers cannot be efficiently resolved (**Fig. 6**).
480 Additionally, our findings establish that DNA effector molecules are pre-loaded into the *cag* T4SS
481 apparatus to establish a 'ready-to-fire' nanomachine that can be rapidly deployed during acute
482 infection, and demonstrate that FtsK is required for partitioning DNA substrates into the *cag* T4SS
483 (**Fig. 6**). Although *H. pylori* harbors several orthologs to paradigmatic DNA conjugation systems,
484 endonucleases, phage integrases, and canonical *A. tumefaciens* VirD2 relaxases, the
485 mechanism by which chromosomally-derived effector DNA is precisely excised and shuttled
486 through the *cag* T4SS while maintaining faithful genome inheritance remains unresolved. Thus,
487 further studies are warranted to explore the intriguing possibility that the *cag* T4SS has co-opted
488 orphaned components of remnant *tfs3* and *tfs4* conjugation systems to enable trans-kingdom
489 DNA delivery (Fernandez-Gonzalez and Backert, 2014).
490
491 Our results provide the first direct evidence that *H. pylori* delivers immunostimulatory
492 chromosomal DNA fragments into target epithelial cells and demonstrate that translocated
493 effector DNA physically binds and activates cytosolic DNA-sensing reconnaissance systems. The
494 observation that chromosomal fragments encompassing full-length eukaryotic genes can be
495 excised and directed to the *cag* T4SS for delivery into target cells underscores the potential to
496 exploit *H. pylori* trans-kingdom conjugation for targeted DNA cargo delivery. Notably, our work
497 provides the essential experimental framework required to harness the *cag* T4SS as a mucosal-

498 targeted DNA vaccine or therapeutic delivery device that can be pharmacologically controlled *in*
499 *vivo*. Studies to determine the maximal DNA fragment length that can be efficiently transported to
500 gastric cells via *cag* T4SS mechanisms are currently underway.
501
502 Our work highlights the importance of understanding host-pathogen conflicts that engage cellular
503 PRR signaling axes to drive chronic inflammation and stimulate the development of infection-
504 related malignancies. While we propose that translocated microbial DNA plays a critical and
505 underappreciated role in the development of inflammation-associated carcinogenesis, further
506 investigations are required to understand STING-dependent outcomes within the context of
507 gastric cancer. Our findings identify a central role of *cag* T4SS activity in eliciting cGAS-STING
508 immunosurveillance in the gastric epithelium; however, additional studies are necessary to
509 understand how STING activation shapes the gastric immune landscape to enable persistent *H.*
510 *pylori* colonization and to elucidate whether STING signaling influences the development of pre-
511 malignant lesions. Finally, our work more broadly points towards therapeutic STING modulation
512 as a promising intervention strategy to reduce the incidence and severity of infection-associated
513 malignancies that arise as a consequence of chronic inflammation.
514
515 **ACKNOWLEDGEMENTS**
516 This work was funded by the NIH (P20 GM130456 and P30 GM110787 to CLS) and academic
517 developments funds provided by the University of Kentucky (to CLS).
518
519 **METHODS**
520 **Bacterial strains and culture conditions.** *Helicobacter pylori* strain 26695, strain G27, isogenic
521 derivatives, and clinical isolates were propagated on trypticase soy agar plates supplemented
522 with 5% sheep blood (BD) as previously described (Shaffer et al., 2011). Overnight cultures of *H.*
523 *pylori* were grown in Brucella broth supplemented with 5% fetal bovine serum (FBS) at 37°C with
524 5% CO_2. For cloning purposes, *E. coli* DH5α (New England Biolabs) were grown on lysogeny
525 broth (LB) agar plates or in LB liquid medium with appropriate antibiotics required for plasmid
526 maintenance.
527
528 **Human cell culture.** The AGS human gastric adenocarcinoma epithelial cell line (ATCC CRL-
529 1739) was cultured in RPMI 1640 medium supplemented with 10% FBS, 2 mM L-glutamine, and
530 10 mM HEPES in the presence of 5% CO_2 at 37°C. Primary adult human gastric epithelial cells
531 (Cell Biologics H-6039) were grown in human epithelial cell medium supplemented with ITS, EGF,
532 hydrocortisone, L-glutamine, and 5% FBS (Cell Biologics H6621) in collagen-coated cell culture
533 flasks at 5% CO_2 and 37°C. Prior to assays, wells of tissue culture plates were coated in collagen
534 following manufacturer's protocol. HEK293-hTLR9 (Invivogen hkb-htlr9), the corresponding
535 parental HEK293 null1 (InvivoGen hkb-null1), HEK293-hTLR7 (Invivogen hkb-htlr7), HEK-
536 Lucia™ hRIG-I (Invivogen hkl-hrigi), and 293T (ATCC CRL-3216) were grown in DMEM
537 supplemented with 10% heat-inactivated FBS and 1X GlutaMAX (Life Technologies) in the
538 presence of 5% CO_2 at 37°C. For cell treatments prior to bacterial challenge, the following
539 compounds were added at the indicated final concentration one hour prior to bacterial challenge:
540 MitoTempo (Sigma-Aldrich, 100 μM); *N*-acetylcysteine (Sigma-Aldrich, 1 mM); BAX-inhibiting
541 peptide, negative control (Sigma-Aldrich, 200 μM); BAX-inhibiting peptide V5 (Sigma-Aldrich, 200
542 μM); or sphingomyelinase inhibitor GW4869 (Sigma-Aldrich, 10 μM).
543
544 ***H. pylori* mutagenesis.** Isogenic mutant derivatives of *H. pylori* 26695 and G27 were generated
545 essentially as previously described (Johnson et al., 2014; Shaffer et al., 2011; Varga et al., 2021).
546 Briefly, *H. pylori* was transformed with a suicide plasmid in which the coding region of the target
547 gene was replaced by either a kanamycin resistance cassette or a chloramphenicol resistance
548 cassette and homologous flanking DNA sequences 500 base pairs (bp) up- and downstream of

549 the target locus. Colonies resistant to kanamycin (12.5 µg/ml) or chloramphenicol (10 µg/ml) were
550 PCR-verified to confirm insertion of the resistance cassette into the appropriate locus. To
551 complement mutants in *cis* at the *ureA* locus, plasmids derived from pAD1 (Shaffer et al., 2011)
552 were constructed to express either the native gene or a hemagglutinin (HA) epitope-tagged
553 protein as previously described (Shaffer et al., 2011; Varga et al., 2021). Plasmid sequences were
554 confirmed by sequencing, and constructs were used to transform isogenic mutant strains.
555 Insertion of complementation constructs into the *ureA* locus was confirmed by PCR amplification
556 and anti-HA immunoblotting, when appropriate.
557
558 To construct *H. pylori* strains harboring NanoLuc luciferase expression constructs, a 1654 bp
559 fragment encompassing the CMV enhancer element, CMV promoter, NanoLuc luciferase gene,
560 and SV40 late poly(A) signal was amplified from pNL1.1.CMV[Nluc/CMV] (19.1 kDa NanoLuc
561 protein, Promega). The PCR product was blunt end ligated to pAD1 digested with EcoRV. Ligation
562 insertion was confirmed by PCR and DNA sequencing. Clones in which the NanoLuc luciferase
563 construct was inserted in the reverse orientation relative to *ureA* transcription were selected for
564 transformation into WT and *cagX H. pylori* 26695 and WT G27 strains. Integrations into the *H.*
565 *pylori* chromosome were confirmed by PCR. The G27 isogenic *cagE* mutant was generated by
566 replacement of the *cagE* coding region with a kanamycin resistance cassette as previously
567 described (Shaffer et al., 2011; Varga et al., 2021). *H. pylori* strains harboring monomeric LifeAct-
568 mScarlet (Bindels et al., 2017) expression constructs were generated using the same
569 mutagenesis strategy, with the exception that a 1872 bp region of pLifeAct_mScarlet-i_N1
570 (Bindels et al., 2017) (26.4 kDa LifeAct-mScarlet protein, Addgene) encompassing the CMV
571 enhancer element, CMV promoter, LifeAct-mScarlet gene, and SV40 late poly(A) signal was
572 amplified was cloned into pAD1 via blunt end ligation. Clones in which the LifeAct mScarlet
573 construct was inserted in the reverse orientation relative to *ureA* transcription were selected for
574 transformation into *H. pylori* 26695 and G27 strains. Integrations into the *ureA* locus were
575 confirmed by PCR.
576
577 **cGAS-STING reporter assays.** 293T cells seeded into 24-well plates at a density of
578 approximately 1.5 x 10^5 cells per well were transfected using Lipofectamine 2000 (Life
579 Technologies) complexed with a combination of plasmids pUNO1-hSTING-R232 (Invivogen
580 puno1-hStingWT), pUNO1-hcGAS-HA3X (Invivogen pUNO1-HA-hcGAS), cGAS derivatives
581 (pUNO1-hcGAS-AA, Invivogen pUNO1-hcGAS-AA; pcDNA3.1-cGAS$_{\Delta DBD}$, Addgene 102606),
582 pRL-SV40P (Addgene 27163), IFN-Beta-pGL3 (Addgene 102597), or empty vector pcDNA3.1
583 (Life Technologies V79020) to ensure equivalent DNA concentrations according to the
584 manufacturer's protocol**.** At 16 h post-transfection, cells were challenged by mid-log phase WT *H.*
585 *pylori,* corresponding *cag* isogenic mutants, or *cag* T4SS+ clinical isolates at a multiplicity of
586 infection (MOI) of 20 bacterial cells per 293T cell. Alternatively, STING reporter cells were
587 transfected with purified *H. pylori* genomic DNA (500 ng/well) at 16 h post-initial transfection of
588 STING and IFN-β reporter plasmids. For cGAS-STING time course assays, *H. pylori* were added
589 to reporter cell monolayers at a MOI of 20, and culture plates were centrifuged at 1,800 x g for 1
590 min to synchronize infections. At the indicated time point, gentamicin was added at a final
591 concentration of 100 µg/ml.
592
593 At 24 h post-infection, cell supernatants were removed, and adherent cells were lysed in
594 luciferase assay passive lysis buffer (Pierce). Luciferase luminescence generated by 20 µl cell
595 lysate per well in a 96-well plate format was recorded with a microplate reader (BioTek Synergy
596 H1) using the Dual-Luciferase Reporter Assay System (Pierce). Firefly luciferase luminescence
597 (D-Luciferin, IFN-Beta-pGL3) was normalized to Renilla luciferase luminescence (coelenterzine,
598 pRL-SV40P) for each well, and IFN-β transcriptional reporter values were expressed as the

599 normalized fold change over mock-infected wells. A minimum of three biological replicate
600 experiments were performed in quadruplicate for each assay.
601
602 To evaluate the requirement of direct bacteria-host cell contact for cGAS-STING signaling, 293T
603 cells were seeded directly into the well of a 24-well plate or into a 0.4 µm pore size transwell insert
604 at approximately 5 x 10^4 cells per transwell. Cells were transfected as described for cGAS-STING
605 reporter cell assays. To physically separate bacterial cells from reporter cells, transfected cGAS-
606 STING reporter cells challenged by the addition of WT *H. pylori* 26695 added to either the apical
607 transwell chamber (293T cells seeded directly into the cell culture well), or the basolateral
608 compartment (293T cells seeded in the transwell apparatus) at a MOI of 20. As a control, cGAS-
609 STING assays in which *H. pylori* were added directly to reporter cell monolayers were performed
610 in parallel. After 24 h of bacterial infection, monolayers were processed as described for cGAS-
611 STING activation assays, and luminescence values were obtained. IFN-β transcriptional reporter
612 values were expressed as the normalized fold change over mock infected wells.
613
614 **STING transactivation assays.** For STING transactivation assays, 293T cells were transfected
615 with either (i) pUNO1-hcGAS-HA3X, pRL-SV40P, and pcDNA3.1 empty vector, or (ii) pUNO1-
616 hSTING-R232, pRL-SV40P, and IFN-Beta-pGL3 using Lipofectamine 2000 as described for
617 cGAS-STING activation assays. At 12 h post-transfection, cells were lifted using sterile phosphate
618 buffered saline (PBS) and were re-plated in 24-well dishes at a 1:1 ratio at approximately 2 x 10^5
619 cells/well. Cells were allowed to adhere and were subsequently challenged by the indicated *H.*
620 *pylori* strain at a MOI of 20. After 24 h of bacterial infection, IFN-β transcriptional reporter activity
621 was assayed as described for cGAS-STING activation experiments. STING transactivation by
622 cGAMP diffusion was expressed as the normalized fold change of IFN-β transcriptional reporter
623 activity over mock infected wells.
624
625 **TLR and RIG-I activation assays.** To assess TLR9 or TLR7 activation, HEK293 stably
626 transfected with hTLR9, hTLR7, or parental null1 cells (Invivogen) were seeded into 96-well plates
627 at a density of approximately 2 x 10^4 cells per well, and were subsequently by WT *H. pylori* 26695
628 or its isogenic mutant strains at a MOI of 100 in quadruplicate as previously described (Varga et
629 al., 2016b; Varga et al., 2021). Supernatants were collected at 24 h post-infection, and TLR9 and
630 TLR7 activation was determined by measuring secreted embryonic alkaline phosphatase (SEAP)
631 reporter activity in cell culture supernatants by QuantiBlue™ reagent (Invivogen) using a
632 microplate reader (BioTek Synergy HI) to record the absorbance at 650 nm. As a positive control
633 for TLR7 activation, HEK293-hTLR7 reporter cells were stimulated with 5 µg/ml imiquimod
634 (R837), an imidazoquinoline amine analog to guanosine (Invivogen). TLR9 or TLR7 activation
635 was normalized to SEAP levels produced by infected null1 parental cells and is expressed as the
636 fold-change over mock infected controls. For ciprofloxacin inhibition of bacterial DNA replication,
637 ciprofloxacin was added to HEK293-hTLR9 co-cultures at the same time as bacterial inoculation
638 at multiples of the previously reported minimum inhibitory concentration (MIC), with 1X MIC
639 equivalent to 0.125 µg/ml. Inhibition of TLR9 activation is expressed as a percent of the
640 normalized fold change over mock treated, *H. pylori*-challenged wells.
641
642 For RIG-I activation studies, HEK-Lucia™ hRIG-I cells were plated in a 96-well dish at
643 approximately 5 x 10^4 cells per well and were subsequently challenged by WT *H. pylori* 26695 or
644 the indicated isogenic mutant strain at a MOI of 100 in quadruplicate. As a positive control, cells
645 were transfected with 100 ng/ml of the RIG-I agonist 5' triphosphate hairpin RNA (3p-hpRNA,
646 Invivogen) complexed to Lipofectamine 2000 (Life Technologies) according to the manufacturer's
647 protocol. At 24 h post-challenge, RIG-I stimulation was assessed by analyzing Lucia luciferase
648 reporter gene expression in 20 µl cell culture supernatants using QUANTI-Luc™ (Invivogen). Data
649 are expressed as the normalized fold change over mock infected cells. TLR and RIG-I stimulation

650 experiments were performed a minimum of three times with quadruplicate technical replicates per
651 experimental condition.
652
653 **CagA translocation assays.** AGS or 293T cells were plated in 12-well dishes at a seeding
654 density of 1 x 10^5 cells/well and were cultured overnight. Monolayers were challenged by the
655 indicated *H. pylori* strain at a MOI of 100 for 6 h, as previously described (Shaffer et al., 2011;
656 Varga et al., 2021). Wells were washed in sterile PBS to remove non-adherent bacteria, and cells
657 were lysed in assay buffer (1% NP-40) supplemented with cOmplete™ mini EDTA-free protease
658 inhibitor (Roche) and PhosSTOP phosphatase inhibitor (Roche). The soluble fraction was
659 collected and prepared in 2X SDS buffer for immunoblotting. To assess CagA tyrosine
660 phosphorylation, AGS or 293T samples were separated on 7.5% gels (Bio-Rad) for 60 min at
661 165V. Proteins were then transferred onto nitrocellulose using the TransBlot Turbo system (Bio-
662 Rad) following manufacturer's recommendations. Membranes were blocked in 3% BSA in Tris-
663 buffered saline containing 0.1% Tween-20 (TBST), followed by incubation with anti-
664 phosphotyrosine monoclonal antibody (α-PY99, Santa Cruz Biotechnology). Total CagA levels
665 were assessed by subsequent incubation with an anti-CagA monoclonal antibody (α-CagA, Santa
666 Cruz Biotechnology). Phosphorylation of CagA or total CagA was visualized using
667 chemiluminescence (Pierce). TEM-CagA translocation was assayed as previously described
668 (Varga et al., 2021).
669
670 **Bacterial adherence and internalization assays.** Adherence and internalization into gastric or
671 kidney epithelial cells were assessed as previously described(Varga et al., 2021). Briefly, WT *H.*
672 *pylori* or the *cagX* isogenic derivative were co-cultured with AGS or 293T cells at a MOI of 100.
673 After a 4 or 6 h infection, respectively, cell culture medium was aspirated, and cell monolayers
674 were gently washed with sterile PBS to remove non-adherent bacteria. To assess intracellular
675 bacteria, RPMI or DMEM supplemented with gentamycin (100 µg/mL) was added to a subset of
676 wells, and the cells were incubated for an additional hour at 37°C in 5% CO_2. To assess total
677 adherent and intracellular bacteria, fresh RPMI or DMEM was replenished into the remainder of
678 wells following the removal of non-adherent bacteria. After the 1 h incubation, RPMI or DMEM
679 was aspirated and all wells were washed in sterile PBS, lysed by mechanical disruption, and were
680 serially diluted on blood agar plates for colony enumeration. Experiments were performed a
681 minimum of three times with triplicate technical replicates per cell line and culture condition.
682
683 **Detection of bacterial DNA in AGS cytosolic extracts.** Digitonin extracts of AGS gastric
684 epithelial cells were prepared essentially as previously described(West et al., 2015). Briefly,
685 approximately 8.4 x 10^6 AGS cells were infected with exponentially growing WT or *cagX H. pylori*
686 at a MOI of 50. As a control, an equivalent number of AGS cells were mock infected. After 6 h of
687 infection, cells were rinsed with sterile PBS and were treated with 50 units of Turbo DNaseI (Life
688 Technologies) in digestion buffer at 37°C for 15 min. The cells were rinsed twice with PBS,
689 trypsinized, and collected in 2 ml of sterile PBS. Collected cells were separated into aliquots of
690 approximately 400 µl to generate 'total' cell extracts, and of approximately 1600 µl to generate
691 'cytosolic' extracts. Aliquots were centrifuged at 980 x g for 3 min and cell pellets were washed
692 once with PBS. To generate the 'total' cell extract, one pellet for was re-suspended in 100 µl of
693 50 µM NaOH and incubated for 30 min at 95°C to solubilize DNA, followed by pH neutralization
694 by the addition of 10 µl of 1 M Tris-HCl, pH 8. These extracts served as normalization controls for
695 the quantitation of mitochondrial DNA (mtDNA) and bacterial DNA. To generate 'cytosolic'
696 extracts, cell pellets were re-suspended in cytosolic extraction buffer (150 mM NaCl, 50 mM Tris
697 pH 8.0, and 20 µg/ml Digitonin [Sigma-Aldrich]), and homogenates were rotated end-over-end for
698 10 min at room temperature for selective membrane permeabilization. Cytosolic fractions were
699 separated from intact cells and nuclear/bacterial fractions by serial centrifugations at 17,000 x g
700 for 3 min. Recovered supernatants were incubated for 10 min at 95°C to isolate DNA. To assess

701 the presence of nuclear DNA, mtDNA, and *H. pylori* DNA in cellular fractions, standard PCR and
702 qPCR targeting fragments of the *H. pylori* chromosome (*hp1421*, 290 bp), mtDNA (*coxII*, 444
703 bp(Fernandez-Moreno et al., 2016)), and nuclear DNA (*hNuc*, 467 bp (Fernandez-Moreno et al.,
704 2016)) were amplified from 'total' and 'cytosolic' fractions using Taq polymerase (standard PCR)
705 or Fast SYBR Green chemistry (qPCR) on a Viia7 platform (Thermo). C_T values obtained for
706 cytosolic fractions were normalized to corresponding C_T values obtained for total cell extracts,
707 and cytosolic enrichment of bacterial DNA was calculated as the normalized ratio of *hp1421* C_T
708 values to *coxII* C_T values. A minimum of four biological replicate experiments were performed for
709 each experimental condition.
710
711 **Quantitation of secreted extracellular cGAMP.** AGS cells seeded into T25 flasks were grown
712 to approximately 80% confluency were mock infected or were challenged by *H. pylori* at a MOI of
713 100 for 6 h. Bacteria were inactivated by the addition of 200 µg/ml gentamicin, and monolayers
714 were incubated overnight. At 24 h post-infection, equivalent volumes of cell culture supernatants
715 were collected and concentrated via solvent evaporation. Samples were reconstituted in one-
716 tenth volume assay buffer, and cGAMP levels were quantified using the DetectX® 2',3'-cGAMP
717 STING-Based FRET assay (Arbor Assays). For each experimental condition, cGAMP secretion
718 assays were performed in triplicate and data represents a minimum of three biological replicates.
719
720 **Confocal laser scanning microscopy.** Adult primary human gastric epithelial cells were grown
721 on collagen-coated 12 mm glass coverslips (#1.5, 170 µm thickness) overnight prior to challenge
722 by WT or *cagX H. pylori* at a MOI of 50. As a control, a subset of coverslips was mock infected.
723 After 6 h, coverslips were washed in sterile PBS three times, followed by fixation in 4%
724 paraformaldehyde in PBS for 20 min at room temperature. Coverslips were washed in PBS and
725 cells were permeabilized in confocal blocking buffer (3% bovine serum albumin, 0.1% TritonX-
726 100, 1% saponin in sterile PBS) for 1 h at room temperature. For immunostaining, coverslips were
727 stained with anti-STING monoclonal antibody (Life Technologies, 1:100) in confocal blocking
728 buffer overnight at 4°C. Coverslips were rigorously washed three times in PBST to remove
729 unbound antibody and were subsequently incubated in AlexaFluor 488-conjugated secondary
730 antibody (Life Technologies, 1:1000) in blocking buffer for 1 h at room temperature. For
731 visualization of the nuclei and actin, samples were stained with stained with 4',6-diamidino-2-
732 phenylindole (DAPI) and AlexaFluor 594 phalloidin for 1 h at room temperature. Coverslips were
733 washed in PBS and were mounted with ProLong Gold antifade (Life Technologies). Fluorescence
734 images were captured using a 60X silicon immersion objective on an Olympus FV3000 confocal
735 laser scanning microscope and images were acquired and processed using cellSens software
736 (Olympus). Quantification of STING particle size and number was performed using Fiji software
737 (ImageJ) with automated thresholding and subsequent particle analysis of segmented images for
738 mock infected (7 fields of view, n=90 cells); WT infected (11 fields of view, n=82 cells); and *cagX*
739 infected (9 fields of view, n=59 cells) gastric epithelial cells. To normalize across imaging
740 conditions, average particle sizes were calculated by multiplying the average pixel area by the
741 pixel resolution for each field of view.
742
743 **RNA isolation and gene expression analyses.** Primary gastric epithelial cells were mock
744 infected (n=3 biological replicates) or co-cultured with WT *H. pylori* 26695 (n=6 biological
745 replicates) or the corresponding *cagX* isogenic mutant (n=3 biological replicates) for 6 h. Cells
746 were washed three times with sterile PBS and total RNA was isolated using the Direct-Zol
747 Miniprep Plus kit (Zymo Research) following the manufacturer's protocol. Total RNA was
748 stringently digested with Turbo DNase I (Invitrogen) to remove contaminant DNA. To determine
749 inflammatory gene expression changes in response to *H. pylori* infection, DNA-free RNA (100 ng
750 per sample) was analyzed on the nCounter Sprint Profiler (NanoString Technologies) using the
751 nCounter Human Host Response Panel (NanoString Technologies), which simultaneously

752 quantifies transcripts for 773 immune-related genes and 12 internal reference genes. Differences
753 in gene expression between experimental groups was calculated using the ROSALIND Platform
754 for nCounter Analysis (https://rosalind.onramp.bio/). Raw data (RCC files) were normalized to
755 internal reference genes the nSolver 4.0 software integrated within the ROSALIND platform
756 (ROSALIND, Inc.). Gene normalization was performed using housekeeping probes selected
757 based on the geNorm algorithm as implemented in the Bioconductor package NormqPCR.
758 Differentially expressed genes in *H. pylori* challenged cells were determined using the Benjamini–
759 Hochberg *P* value adjustment method of estimating false discovery rates (FDR), with significance
760 set at $p<0.05$. Read distribution percentages, violin plots, identity heatmaps, and sample
761 multidimensional scaling (MDS) plots were generated within ROSALIND during sample QC. Read
762 normalization, gene expression fold changes, and the associated *P* values were calculated using
763 criteria provided by NanoString. Pathway enrichment analysis was performed within ROSALIND
764 using the REACTOME database, and gene term enrichment was calculated using a
765 hypergeometric distribution algorithm in reference to the background set of genes in the panel
766 with significance set at $p<0.01$ and greater than $\pm$ 1.8-fold gene expression enrichment. Volcano
767 plots and heat maps were generated in GraphPad Prism using normalized gene expression data
768 exported from ROSALIND. Volcano plots were constructed by plotting the $\log_2$ of the normalized
769 fold change versus the $-\log_{10}$ of the adjusted *P* value for each gene. The dashed P_{adj} lines
770 demarcate genes meeting the threshold for significance ($P_{adj}<0.01$ and $P_{adj}<0.05$) after correction
771 with the Benjamini–Hochberg procedure for controlling FDR.
772
773 **Gastric epithelial cell supernatant transfer assay.** Primary gastric epithelial cells seeded into
774 24-well gelatin-coated dishes were mock infected or were co-cultured with WT *H. pylori* or the
775 *cagX* isogenic mutant at a MOI of 100 for 6 h or 12 h. Cell culture supernatants were harvested
776 and treated with 100 µg/ml gentamicin for 1 h at 37°C to eliminate viable bacteria. Supernatants
777 were subsequently spun for 10 min at 10,000 x g to remove bacteria and gastric cells, and cleared
778 supernatants were stored at -20°C. For TLR9 stimulation studies, HEK293-hTLR9 cells were
779 seeded into 96-well plates at a density of approximately 2 x 10^4 cells per well in a volume of 100
780 µl DMEM per well. Primary gastric epithelial cell supernatants were added to hTLR9 reporter cells
781 at an equal volume and incubated for 24 h at 37°C in 5% CO_2. TLR9 activation was determined
782 via SEAP levels determined by QuantiBlue™ (Invivogen) using a microplate reader (BioTek
783 Synergy HI) to record the absorbance at 650 nm. The concentration of cell-free DNA in processed
784 supernatants was determined by high sensitivity dsDNA Qubit assay (Life Technologies).
785
786 For enzyme treatments of gastric epithelial cell supernatants, pre-cleared supernatants obtained
787 from 6 h *H. pylori* challenged gastric epithelial cells were either treated by (i) the addition of 10
788 units Turbo DNase (Life Technologies) and incubation at 37°C for 30 min, (ii) heating the
789 supernatant to 70°C for 15 min, or (iii) heating the supernatant to 70°C for 15 min followed by
790 cooling to room temperature and subsequent DNase treatment as described in (i). Treated
791 supernatants were added to HEK293-hTLR9 reporter cells as described for supernatant transfer
792 assays, and TLR9 stimulation was assessed by QuantiBlue™ after 24 h incubation. TLR9
793 activation is expressed as the fold change over mock treated HEK293-hTLR9 cells.
794
795 **Extracellular vesicle (EV) purification.** Primary gastric epithelial cells were challenged by *H.*
796 *pylori* or were mock infected for 6 h. Supernatants were pre-cleared by serial centrifugations
797 (10,000 x g) at 4°C. EV-containing supernatants (2 ml per biological replicate) were subsequently
798 magnetically labeled for 1 h at room temperature by CD9, CD63, and CD81 antibodies (Human
799 Exosome Isolation Kit, Pan, Miltenyi Biotec) followed by EV isolation via magnetic separation and
800 elution. Immunoaffinity purified exosomes were subjected to qPCR analysis probing for *H. pylori*
801 genomic DNA (*hp1421* locus, 290 bp fragment) and mtDNA (*coxII*, 444 bp fragment) by Fast
802 SYBR Green chemistry (Life Technologies) on a Viia7 platform (Thermo). *H. pylori* DNA

803 enrichment within purified EVs was determined by quantifying the ratio of *hp1421* C_T values to
804 *coxII* C_T values for EVs obtained from WT and *cagX*-infected gastric cells. EVs purified from mock
805 infected gastric epithelia contained levels of mtDNA similar to EVs derived from *H. pylori*-
806 challenged primary cells.
807
808 **Immunoprecipitation of cGAS-DNA complexes.** 293T cells were grown in 6-well plates for 24-
809 30 hours to achieve approximately 90% confluency. Cells were transfected with pUNO1-hcGAS-
810 HA3X (240 ng DNA/well) complexed to Lipofectamine 2000. After 12 – 16 h, approximately 7.2 x
811 10^6 transfected 293T cells were challenged by exponentially growing WT or *cagX H. pylori* at a
812 MOI of 100. As a control, an equivalent number of transfected 293T cells were mock infected.
813 After 6 h of infection, 293T cells were rinsed with PBS and DNA-protein complexes were cross-
814 linked by 1% paraformaldehyde for 15 min at room temperature. Cross-linking reactions were
815 quenched by the addition of 250 mM glycine, and cells were collected by mechanical detachment
816 and centrifugation at 4000 rpm for 10 min. Cell pellets were washed once with sterile PBS,
817 followed by re-suspension in pre-chilled lysis buffer (5 mM EDTA, 1% NP-40, and 1X protease
818 inhibitor cocktail in PBS) and sonication at 5% amplitude (10 Sec ON, 10 Sec OFF, 4-6 cycles) to
819 generate cleared lysates. Sonicated cell extracts were centrifuged at 14,000 rpm for 30 min at
820 4°C. The recovered cell-free supernatant was incubated with 4 µg of anti-HA monoclonal
821 antibodies (clone 12CA5) overnight at 4°C with continuous end-over-end rotation. The following
822 day, 50 µl of Protein G Dynabeads (Life Technologies) pre-blocked in PBS containing 1% BSA
823 were incubated with immunopurification samples for 90-120 min at 4°C with continuous end-over-
824 end rotation. Dynabeads were collected by magnetic isolation, washed twice with 1X cell lysis
825 buffer, followed by one wash in high salt wash buffer (cell lysis buffer + 300 mM NaCl). Magnetic
826 beads were re-suspended in 100 µl of 1% SDS + 0.1 M sodium bicarbonate buffer and de-
827 crosslinked by incubation at 60°C overnight. Purification of cGAS-HA3x was confirmed in the
828 eluted fractions by immunoblot analysis. To purify DNA complexed with cGAS-HA3x, de-
829 crosslinked fractions were treated with 20 µg of Proteinase K (Sigma-Aldrich) at 60°C for 1-2 h,
830 followed by DNA isolation via the ChIP DNA Clean and concentrator kit (Zymo Research)
831 according to the recommended protocol. Eluted DNA was quantified using the Qubit high
832 sensitivity dsDNA assay (Life Technologies).
833
834 **cGAS 'ChIP-seq' library preparation and sequencing.** ChIP samples were quantified using
835 Qubit 2.0 Fluorometer (Life Technologies) the DNA integrity was analyzed with 4200 TapeStation
836 (Agilent Technologies). cGAS 'ChIP-seq' library preparation and sequencing reactions were
837 conducted at GENEWIZ, Inc. (South Plainfield, NJ, USA). NEB NextUltra DNA Library Preparation
838 kit was used following the manufacturer's recommendations (Illumina). Briefly, DNA eluted from
839 cGAS immunopurifications was end repaired and adapters were ligated after adenylation of the
840 3' ends. Adapter-ligated DNA was size selected, followed by clean up, and limited cycle PCR
841 enrichment. The cGAS 'ChIP' library was validated using Agilent TapeStation and quantified using
842 Qubit 2.0 Fluorometer as well as RT-PCR (Applied Biosystems). Sequencing libraries were
843 multiplexed and clustered on two lanes of a flowcell. After clustering, the flowcell was loaded on
844 the Illumina HiSeq instrument according to manufacturer's protocol (Illumina). Sequencing was
845 performed using a 2x150 paired end (PE) configuration. Image analysis and base calling were
846 conducted by the HiSeq Control Software (HCS). Raw sequence data generated from Illumina
847 HiSeq was converted into fastq files and de-multiplexed using Illumina's bcl2fastq 2.17 software.
848 One mismatch was allowed for index sequence identification. Sequence reads were processed
849 to remove adapter sequences and nucleotides with poor quality at both 5' and 3' ends using CLC
850 Genomics workbench. Sequence reads below 15 bases were discarded. Trimmed data was
851 aligned to both human (*Homo sapiens* reference genome hg38) and *H. pylori* 26695 (reference
852 genome NC_000915) reference genomes. Only specific alignment was allowed during mapping.
853 To detect peaks that were differentially present in cGAS purifications obtained from WT-infected

854 cells versus *cagX*-infected cells, reads were normalized to mock infected control preparations,
855 and peak calling was performed using the Transcription Factor model within CLC Genomics
856 workbench with $p<0.01$ considered significant.
857
858 **Nanoluciferase (NanoLuc) bioluminescence assays.** AGS or 293T cells were cultured
859 overnight to reach approximately 70% confluence, and were challenged by WT or *cagX H. pylori*
860 [NanoLuc] (26695) or WT or *cagE H. pylori* [NanoLuc] (G27) at a MOI of 50 for 24 h. Cell culture
861 supernatants were removed and monolayers were washed in sterile PBS to remove non-adherent
862 cells. Monolayers were lysed in 1% NP-40, and 50 µl of cell lysate was transferred to a white
863 walled 96-well plate. To measure nanoluciferase bioluminescence, 20 µl Nano-Glo Luciferase
864 substrate assay buffer containing furimazine (Promega) prepared according to the manufacturer
865 protocol was added to each well. Luciferase activity was immediately assessed using a BioTek
866 Synergy H1 plate reader with luminesce acquisition settings set as recommended by the
867 manufacturer, with the exception of the gain which was adjusted to 230. To determine the level
868 of background NanoLuc activity produced by *H. pylori*, 20 µl of overnight bacterial cultures were
869 directly lysed in Nano-Glo Luciferase substrate assay buffer containing furimazine, and luciferase
870 values were immediately obtained via plate reader using the same parameters as for eukaryotic
871 cells. Background luminescence produced by *H. pylori* was determined by normalizing luciferase
872 values by the corresponding culture OD_{600} and is expressed as the fold change in luminescence
873 over values obtained for *H. pylori* cultures that do not harbor the nanoluciferase expression
874 construct. Bioluminescence of *H. pylori*-challenged wells is expressed as the fold change over
875 mock infected wells. For each eukaryotic cell line, a minimum of four biological replicate
876 experiments were performed in 24-well plate technical replicate format.
877
878 **Live cell fluorescence microscopy analysis of LifeAct-mScarlet.** *H. pylori* harboring LifeAct-
879 mScarlet constructs were grown to exponential phase in broth culture and AGS or 293T
880 monolayers were inoculated at a MOI of 50 overnight at 37°C in 5% CO_2. Monolayers were
881 washed in sterile PBS to remove non-adherent bacteria, and monolayers were imaged via live
882 cell, phase contrast epi-fluorescence microscopy on a Nikon Ti Eclipse equipped with a 594_{em}
883 filter and a Plan Apo VC 20X/0.75 NA air objective. Fluorescent images were superimposed on
884 the corresponding phase contrast image of the same field of view. Images were processed for
885 equivalent contrast, brightness, and magnification using the OMERO platform (Allan et al., 2012).
886
887 **Flow cytometry analysis.** AGS or 293T cells were cultured overnight to reach approximately
888 70% confluence, and were challenged by WT or *cagX H. pylori* [LifeAct-mScarlet] at a MOI of 50
889 for 24 h. Cell culture supernatants were removed and monolayers were washed in sterile PBS to
890 remove non-adherent cells. Cells were trypsinized (AGS) or mechanically detached (293T) from
891 tissue culture flasks, washed once in PBS via centrifugation and pelleting, and re-suspended in
892 PBS at approximately 1 x 10^6 cells/ml. Samples were analyzed on an Attune™ NxT Flow
893 Cytometer (Thermo). Forward scatter-height (FSC-H) and sideward scatter-height (SSC-H)
894 profiles were used in gating strategies to select for single cells, and positive mScarlet fluorescence
895 gates were determined by analyzing 293T cells that had been transfected with pLifeAct_mScarlet-
896 i_N1 (Bindels et al., 2017).
897
898 **IL-8 quantitation.** Interleukin-8 (IL-8) secretion was monitored by human CXCL8 ELISA (R&D
899 Systems) as previously described(Shaffer et al., 2011; Varga et al., 2021). Briefly, AGS cells were
900 plated in 24-well dishes and were cultured overnight prior to infection with *H. pylori* at a MOI of
901 100 for 4.5 h. Supernatants were collected and stored at -20°C until analysis by ELISA. A
902 minimum of three biological replicate experiments were performed in triplicate for all strains, and
903 IL-8 secretion is expressed as a percent of IL-8 levels induced by WT *H. pylori* for each replicate
904 experiment.

905
906 **'Transfer DNA' immunoprecipitation.** To assess whether processed chromosomal DNA
907 fragments physically associate with the *cag* T4SS outer membrane complex, *H. pylori* grown for
908 24 h on blood agar were harvested in 2 ml PBS, and 50 µL of the cell suspension were removed
909 to serve as the 'input'. The remainder of the collected cells were pelleted by centrifugation and
910 were washed once in PBS. Cell pellets were re-suspended in 500 µL PBS, and protein-DNA
911 complexes were cross-linked by the addition of 500 µL 1% paraformaldehyde for 10 min at room
912 temperature, followed by quenching with 1 ml 250 mM glycine. Cross-linked cells were pelleted
913 and washed once with PBS. Cell pellets were re-suspended in 1 mL lysis buffer (5 mM EDTA, 1%
914 NP-40 in PBS) supplemented with 2X cOmplete™ inhibitor (Roche) and were sonicated until the
915 lysate became turbid. Cell lysates were treated with 2 units of Turbo DNase (Life Technologies)
916 in 10 mM $MgCl_2$ for 30 min at room temperature. To solubilize membranes, 0.2% SDS and 0.2%
917 sodium deoxycholic acid (final concentrations) were added to cell lysates, and samples were
918 rotated end-over-end for 1-2 h. Supernatants were separated from insoluble cell debris by
919 centrifugation at 14,000 rpm for 30 minutes at 4˚C. In a separate tube, 4 µl polyclonal anti-CagY
920 antisera (a kind gift from Dr. Tim Cover) was added to 800 µl lysis buffer containing 10 mM $MgCl_2$,
921 2 units Turbo DNase, and 25 µl Protein G Dynabeads, and was incubated for 10 min at room
922 temperature. Cleared supernatants were added directly to CagY antibody solutions and were
923 incubated for an additional 2-4 h with continuous end-over-end rotation. Beads were isolated by
924 magnetic separation and were washed twice in PBS supplemented with 10 mM $MgCl_2$ and 1 unit
925 Turbo DNase, followed by two washes in high salt buffer (lysis buffer containing 400 mM NaCl),
926 and a final wash in PBS. Protein-DNA complexes were eluted and de-cross-linked in 100 µl 1%
927 SDS in 0.1 M $NaHCO_3$ at 65˚C overnight. The following day, proteins were digested using
928 Proteinase K (10 µg) at 65˚C for 30 minutes. DNA was precipitated by 100% ethanol in 0.3 M
929 sodium acetate (1:3 v/v) at -20˚C. Precipitated DNA was pelleted by centrifugation at 14,000 rpm
930 for 30 minutes at 4˚C, washed once with 70% ethanol, and re-hydrated in 20 µl ultrapure water.
931 To serve as a control, the initial 'input' cell pellet was re-suspended in 100 µl of 50 µM NaOH, and
932 DNA was liberated by incubating at 95˚C 30 min, followed by pH neutralization by the addition of
933 10 µl of 1M Tris, pH 8. To assess chromosomal DNA association with immunopurified CagY
934 complexes, 1 µl of 'input' and 'IP' DNA samples were used as the template in standard PCR
935 assays targeting a 795 bp chromosomal DNA amplicon. Quantitation of DNA amplification from
936 'input' and 'IP' samples was conducted by densitometry analysis and amplification efficiency of
937 'IP' samples was calculated as a percent of the corresponding 'input' sample amplification for
938 each biological replicate experiment. Transfer DNA immunopurification assays were performed a
939 minimum of four times per strain.
940
941 **Statistical analyses.** Data are expressed as mean values ± standard error of the mean, which
942 were calculated from a minimum of three biological replicate experiments. In all graphs, each data
943 point represents an individual measurement, lines represent the mean, and error bars represent
944 the standard error of the mean. Statistical analyses were performed using GraphPad Prism 9
945 software, with differences of $p<0.05$ considered statistically significant.
946
947 **FIGURE LEGENDS**
948 **Figure 1. *H. pylori cag* T4SS activity stimulates multiple DNA surveillance systems. A**. TLR9
949 activation induced by the indicated *H. pylori* 26695 isogenic mutant strain. Data are expressed as
950 the normalized fold change over mock infected cells. **B**. TLR9 activation requires a functional *cag*
951 T4SS. **C**. cGAS-STING signaling stimulated by the indicated strain. **D**. Induction of double-
952 stranded DNA breaks in the host genome does not significantly contribute to *H. pylori*-induced
953 cGAS-STING signaling. Graph depicts IFN-β reporter activity induced in cGAS-STING reporter
954 cells by the indicated strain. **E**. Transwell cGAS-STING activation assays demonstrating the
955 requirement for direct bacteria-host cell contact. **F**. STING transactivation assays providing

956 evidence of intercellular cGAMP transfer. Schematic depicts the reporter cell line experimental
957 strategy. **G**. IFN-β transcriptional reporter assays demonstrating the requirement of the cGAS
958 DNA-binding domain ($cGAS_{\Delta DBD}$) and cGAS catalytic activity ($cGAS_{\Delta NTase}$) for *H. pylori*-induced
959 cGAS-STING signaling. **H.** cGAS-STING signaling induced by the indicated *H. pylori* strain
960 stratified by disease state (gastritis, duodenal ulcer, and gastric adenocarcinoma). In **A**-**G**,
961 significance was determined by one-way ANOVA with Dunnett's post-hoc correction for multiple
962 comparisons to experimental controls. In all panels, ****, $p<0.0001$.
963
964 **Figure 2. *H. pylori* DNA is delivered to the gastric epithelial cell cytoplasm in a *cag* T4SS-**
965 **dependent manner. A**. Representative PCR amplifications demonstrating the presence of
966 chromosomal *H. pylori* (*hp1421*), nuclear genomic (*hNuc* (Fernandez-Moreno et al., 2016)), and
967 mitochondrial (*coxII* (Fernandez-Moreno et al., 2016)) DNA fragments in fractionated cytoplasmic
968 (C) and total (T) co-culture AGS cell extracts. **B**. qPCR analysis of *H. pylori* DNA enrichment in
969 cytosolic fractions normalized to levels of cytosolic mitochondrial DNA. Results are representative
970 of at least 4 biological replicate experiments. Significance was determined by unpaired, two-tailed
971 t-test; **, $p<0.01$. **C**. Levels of extracellular cGAMP produced by AGS cells in response to *H.*
972 *pylori*. **D**. Confocal microscopy analysis of perinuclear STING localization in *H. pylori*-challenged
973 primary gastric epithelial cells at 6 h post-infection. Representative image of $n=2$ biological
974 replicate experiments depicting STING (green), nuclei (blue), and actin (magenta) staining. Scale
975 bar represents 20 µm. **E**. Quantitation of STING particle size in primary gastric epithelial cells
976 challenged by the indicated *H. pylori* strain. Data represents the average STING particle size per
977 field of view for mock infected (7 fields of view, $n=90$ cells); WT infected (11 fields of view, $n=82$
978 cells); and *cagX* infected (9 fields of view, $n=59$ cells) gastric epithelial cells. **F**. STING signaling
979 induced by the indicated *H. pylori* strain or purified *H. pylori* chromosomal DNA in 293T reporter
980 cells. Data is representative of a minimum of 3 biological replicate experiments. In **E-F**,
981 significance was determined by one-way ANOVA with Dunnett's post-hoc correction for multiple
982 comparisons to experimental controls; ****, $p<0.0001$.
983
984 **Figure 3. *H. pylori* regulates nucleic acid reconnaissance pathways via *cag* T4SS activity.**
985 **A.** Volcano plot depicting expression of immune-related genes in adult human primary epithelial
986 cells challenged by *H. pylori* detected with the NanoString human host response panel. Graph
987 represents the fold change and associated *p*-value of all differentially expressed genes in the
988 panel for WT vs. *cagX* challenged cells. Dashed lines dashed lines demarcate genes meeting the
989 threshold for significance ($p_{adj}<0.01$ and $p_{adj}<0.05$) after correction with the Benjamini–Hochberg
990 procedure for controlling FDR. Selected genes encoding nucleic acid sensing pathways,
991 interferon-responsive elements, and inflammatory cytokines/chemokines are labeled and
992 indicated in pink. **B**. Heat map of differentially expressed genes depicted in a. Map depicts genes
993 that were increased or decreased by 1.8-fold and an adjusted *p*-value <0.01. **C**. Pathway analysis
994 of differentially expressed immune genes. Graph depicts the $-\log_{10}$ *p*-value for the indicated
995 pathway. **D**. TLR7 activation levels induced by the indicated strain or pharmacological stimulus.
996 **E**. Levels of RIG-I signaling stimulated by *H. pylori* or transfected RNA agonist. In **D** and **E**,
997 significance was determined by one-way ANOVA with Dunnett's post-hoc correction for multiple
998 comparisons to experimental controls; ****, $p<0.0001$. Data is derived from $n=1$ NanoString
999 analysis with gastric epithelial cell samples derived from $n=2$ biological replicate experiments
1000 (mock infected, $n=3$, WT infected $n=6$, and *cagX* infected $n=3$ samples analyzed).
1001
1002 **Figure 4. *H. pylori* effector DNA is packaged into exosomes to enable DNA pattern**
1003 **recognition receptor signaling in bystander cells. A**. TLR9 stimulation induced by
1004 supernatants obtained from primary gastric epithelial cells challenged by *H. pylori* at the indicated
1005 time point post-infection. Graph depicts levels of TLR9 activation achieved by supernatants
1006 collected in a minimum of four biological replicate experiments. **B**. Linear regression analysis

1007 revealing no correlation between levels of TLR9 activation induced by gastric epithelial cell
1008 supernatants and the corresponding level of supernatant total cell-free DNA. **C**. Levels of TLR9
1009 activation achieved by gastric cell supernatants obtained at 6 h post-infection and processed by
1010 the indicated conditions. **D**. Induction of TLR9 stimulation by gastric cell supernatant extracellular
1011 vesicles in gastric epithelial cell supernatants challenged by *H. pylori* in the presence or absence
1012 of GW4869 (10 μM). Significance was determined by unpaired, two-tailed t-test; ****, $p<0.0001$.
1013 **E**. qPCR analysis of *H. pylori* DNA enrichment in purified exosomes derived from primary gastric
1014 epithelial co-culture supernatants 6 h post-bacterial challenge by the indicated strain. Graph
1015 depicts the fold enrichment of *H. pylori* DNA (*hp1421*) over levels of mitochondrial DNA (*coxII*) in
1016 exosomes purified from supernatants collected from five biological replicate experiments.
1017 Significance was determined by unpaired, two-tailed t-test; **, $p<0.01$. **F**. Schematic representing
1018 a proposed model of translocated *H. pylori* DNA packaging and subsequent release of
1019 extracellular vesicles by primary gastric cells. In **A** and **C**, significance was determined by one-
1020 way ANOVA with Dunnett's post-hoc correction for multiple comparisons to experimental controls;
1021 ****, $p<0.0001$, ***, $p<0.001$, and **, $p<0.01$.
1022
1023 **Figure 5. Chromosomally-derived DNA is translocated into target cells via *cag* T4SS**
1024 **mechanisms. A**. Merged tracks of mapped *H. pylori* DNA reads obtained from infected 293T
1025 cGAS cells. Graph depicts sequencing read depth versus nucleotide position in the *H. pylori*
1026 26695 genome. Schematic illustrates the experimental workflow for cGAS 'ChIP-seq' studies. **B**.
1027 DNA reads co-purified with cGAS were normalized to reads obtained from mock infected cells,
1028 and peak calling was used to identify regions of bacterial DNA that were enriched with cGAS
1029 immunopurification. Dots depict individual peaks and the corresponding peak center on the *H.*
1030 *pylori* 26695 chromosome obtained from WT (purple dots) and *cagX* (maroon dots) challenged
1031 co-cultures. **C**. Schematic of eukaryotic-optimized nanoluciferase expression constructs inserted
1032 into the *hp0073* locus. Nanoluciferase constructs were inserted frameshifted in the opposite
1033 orientation of the native operon transcription. **D**,**E**. Nanoluciferase bioluminescence produced by
1034 AGS (**D**) and 293T (**E**) cells challenged by the indicated strain at 24 h post-infection. Data
1035 represent a minimum of four biological replicate experiments. Significance was determined by
1036 unpaired, two-tailed t-test; **, $p<0.01$. **F,G**. Live cell phase contrast and fluorescence microscopy
1037 analysis of AGS (**F**) and 293T (**G**) cells challenged by WT *H. pylori* harboring LifeAct-mScarlet
1038 expression constructs at 24 h post-infection. Images are representative of $n=2$ biological replicate
1039 experiments. **H-K**. Flow cytometry analysis of AGS (**H** and **I**) or 293T cells (**J** and **K**) challenged
1040 by WT[mScarlet] or *cagX*[mScarlet] at 18 h post-infection. Green boxes indicate gating of
1041 mScarlet positive cells. Data is representative of $n=2$ biological replicate experiments.
1042
1043 **Figure 6. DNA translocation is mechanistically coupled to chromosomal replication and**
1044 **replichore decatenation. A**. TLR9 activation induced by WT *H. pylori* in the presence of the
1045 indicated ciprofloxacin minimum inhibitory concentration (1X MIC = 0.125 μg/ml). Data are
1046 expressed as a percent of TLR9 stimulation achieved by WT in mock treated wells. **B**. Levels of
1047 TLR9 activation induced by the indicated isogenic mutant. Data are expressed as a percent of
1048 TLR9 stimulation achieved by the parental WT strain. **C**. IL-8 secreted by AGS cells challenged
1049 by the indicated *H. pylori* strain at 4.5 h post-infection. Data are expressed as a percent of IL-8
1050 levels stimulated by the corresponding WT strain. **D**. cGAS-STING signaling induced by the
1051 indicted strain. Graph depicts the results of $n=3$ biological replicate experiments. **E**. Transfer DNA
1052 immunopurification assays demonstrating the presence of *H. pylori* chromosomal DNA fragments
1053 within the *cag* T4SS apparatus. Graph depicts the amplification efficiency of a 795 bp fragment in
1054 transfer DNA assay preparations purified from the indicated strain. Amplification efficiency of the
1055 immunopurification (IP) samples are expressed as the percent of the input DNA from at least four
1056 biological replicate experiments. Inset depicts representative PCR amplifications obtained from
1057 input and IP samples prepared from the indicated strain. **F**. Proposed model of DNA cargo

1058 segregation for *cag* T4SS-dependent delivery to host cells. We hypothesize that FtsK-XerH
1059 complexes mediate the rare excision of DNA arising from overlapping rounds of chromosomal
1060 replication for subsequent coupling to the *cag* T4SS apparatus for delivery to host cells. In **A**-**E**,
1061 significance was determined by one-way ANOVA with Dunnett's post-hoc correction for multiple
1062 comparisons to experimental controls; ****, $p<0.0001$ in all panels.

1063 **REFERENCES**

1064 Ablasser, A., Bauernfeind, F., Hartmann, G., Latz, E., Fitzgerald, K.A., and Hornung, V. (2009).
1065 RIG-I-dependent sensing of poly(dA:dT) through the induction of an RNA polymerase III-
1066 transcribed RNA intermediate. *Nature Immunol 10*, 1065-1072.
1067 Ablasser, A., Goldeck, M., Cavlar, T., Deimling, T., Witte, G., Rohl, I., Hopfner, K.P., Ludwig, J.,
1068 and Hornung, V. (2013). cGAS produces a 2'-5'-linked cyclic dinucleotide second
1069 messenger that activates STING. *Nature 498*, 380-384.
1070 Allan, C., Burel, J.M., Moore, J., Blackburn, C., Linkert, M., Loynton, S., Macdonald, D., Moore,
1071 W.J., Neves, C., Patterson, A.*, et al.* (2012). OMERO: flexible, model-driven data
1072 management for experimental biology. *Nat Methods 9*, 245-253.
1073 Almine, J.F., O'Hare, C.A., Dunphy, G., Haga, I.R., Naik, R.J., Atrih, A., Connolly, D.J., Taylor, J.,
1074 Kelsall, I.R., Bowie, A.G.*, et al.* (2017). IFI16 and cGAS cooperate in the activation of
1075 STING during DNA sensing in human keratinocytes. *Nat Commun 8*, 14392.
1076 Amieva, M., and Peek, R.M. (2016). Pathobiology of *Helicobacter pylori*-induced gastric cancer.
1077 *Gastroenterology 150*, 64-78.
1078 Bauer, M., Nascakova, Z., Mihai, A.I., Cheng, P.F., Levesque, M.P., Lampart, S., Hurwitz, R.,
1079 Pfannkuch, L., Dobrovolna, J., Jacobs, M.*, et al.* (2020). The ALPK1/TIFA/NF-kappaB axis
1080 links a bacterial carcinogen to R-loop-induced replication stress. *Nat Commun 11*, 5117.
1081 Bebel, A., Karaca, E., Kumar, B., Stark, W.M., and Barabas, O. (2016). Structural snapshots of
1082 Xer recombination reveal activation by synaptic complex remodeling and DNA bending.
1083 *Elife 5*.
1084 Bindels, D.S., Haarbosch, L., van Weeren, L., Postma, M., Wiese, K.E., Mastop, M., Aumonier,
1085 S., Gotthard, G., Royant, A., Hink, M.A.*, et al.* (2017). mScarlet: a bright monomeric red
1086 fluorescent protein for cellular imaging. *Nat Methods 14*, 53-56.
1087 Boxx, G.M., and Cheng, G. (2016). The roles of type I interferon in bacterial infection. *Cell Host*
1088 *Microbe 19*, 760-769.
1089 Cai, X., Chiu, Y.H., and Chen, Z.J. (2014). The cGAS-cGAMP-STING pathway of cytosolic DNA
1090 sensing and signaling. *Molecular Cell 54*, 289-296.
1091 Callaghan, M.M., Heilers, J.H., van der Does, C., and Dillard, J.P. (2017). Secretion of
1092 chromosomal DNA by the *Neisseria gonorrhoeae* type IV secretion system. *Current Top*
1093 *Microbiol Immunol 413*, 323-345.
1094 Carozza, J.A., Bohnert, V., Nguyen, K.C., Skariah, G., Shaw, K.E., Brown, J.A., Rafat, M., von
1095 Eyben, R., Graves, E.E., Glenn, J.S.*, et al.* (2020). Extracellular cGAMP is a cancer cell-
1096 produced immunotransmitter involved in radiation-induced anti-cancer immunity. *Nat*
1097 *Cancer 1*, 184-196.
1098 Castano-Rodriguez, N., Kaakoush, N.O., and Mitchell, H.M. (2014). Pattern-recognition receptors
1099 and gastric cancer. *Front Immunol 5*, 336.
1100 Chaturvedi, R., Asim, M., Piazuelo, M.B., Yan, F., Barry, D.P., Sierra, J.C., Delgado, A.G., Hill,
1101 S., Casero, R.A., Jr., Bravo, L.E.*, et al.* (2014). Activation of EGFR and ERBB2 by
1102 *Helicobacter pylori* results in survival of gastric epithelial cells with DNA damage.
1103 *Gastroenterology 146*, 1739-1751 e1714.
1104 Chen, S., Bonifati, S., Qin, Z., St Gelais, C., Kodigepalli, K.M., Barrett, B.S., Kim, S.H., Antonucci,
1105 J.M., Ladner, K.J., Buzovetsky, O.*, et al.* (2018). SAMHD1 suppresses innate immune
1106 responses to viral infections and inflammatory stimuli by inhibiting the NF-kappaB and
1107 interferon pathways. *Proc Nat Acad Sci USA 115*, E3798-E3807.
1108 Chiu, Y.H., Macmillan, J.B., and Chen, Z.J. (2009). RNA polymerase III detects cytosolic DNA
1109 and induces type I interferons through the RIG-I pathway. *Cell 138*, 576-591.
1110 Chow, J., Franz, K.M., and Kagan, J.C. (2015). PRRs are watching you: Localization of innate
1111 sensing and signaling regulators. *Virology 479-480*, 104-109.

1112 Chung, J.M., Sheedlo, M.J., Campbell, A.M., Sawhney, N., Frick-Cheng, A.E., Lacy, D.B., Cover,
1113 T.L., and Ohi, M.D. (2019). Structure of the *Helicobacter pylori* cag type IV secretion
1114 system. *Elife 8*.
1115 Cover, T.L., Lacy, D.B., and Ohi, M.D. (2020). The *Helicobacter pylori cag* type IV secretion
1116 system. *Trend Microbiol 28*, 682-695.
1117 Das, A., Dinh, P.X., Panda, D., and Pattnaik, A.K. (2014). Interferon-inducible protein IFI35
1118 negatively regulates RIG-I antiviral signaling and supports vesicular stomatitis virus
1119 replication. *J Virol 88*, 3103-3113.
1120 Debowski, A.W., Carnoy, C., Verbrugghe, P., Nilsson, H.O., Gauntlett, J.C., Fulurija, A., Camilleri,
1121 T., Berg, D.E., Marshall, B.J., and Benghezal, M. (2012). Xer recombinase and genome
1122 integrity in *Helicobacter pylori*, a pathogen without topoisomerase IV. *PLoS One 7*,
1123 e33310.
1124 Diner, E.J., Burdette, D.L., Wilson, S.C., Monroe, K.M., Kellenberger, C.A., Hyodo, M., Hayakawa,
1125 Y., Hammond, M.C., and Vance, R.E. (2013). The innate immune DNA sensor cGAS
1126 produces a noncanonical cyclic dinucleotide that activates human STING. *Cell Rep 3*,
1127 1355-1361.
1128 Dixit, E., and Kagan, J.C. (2013). Intracellular pathogen detection by RIG-I-like receptors. *Adv*
1129 *Immunol 117*, 99-125.
1130 Fernandez-Gonzalez, E., and Backert, S. (2014). DNA transfer in the gastric pathogen
1131 *Helicobacter pylori*. *J Gastroenterol 49*, 594-604.
1132 Fernandez-Moreno, M., Hermida-Gomez, T., Gallardo, M.E., Dalmao-Fernandez, A., Rego-
1133 Perez, I., Garesse, R., and Blanco, F.J. (2016). Generating Rho-0 cells using
1134 mesenchymal stem cell lines. *PLoS One 11*, e0164199.
1135 Frick-Cheng, A.E., Pyburn, T.M., Voss, B.J., McDonald, W.H., Ohi, M.D., and Cover, T.L. (2016).
1136 Molecular and structural analysis of the *Helicobacter pylori cag* type IV secretion system
1137 core complex. *mBio 7*.
1138 Gall, A., Gaudet, R.G., Gray-Owen, S.D., and Salama, N.R. (2017). TIFA signaling in gastric
1139 epithelial cells initiates the *cag* type 4 secretion system-dependent innate immune
1140 response to *Helicobacter pylori* infection. *mBio 8*.
1141 Gao, D., Li, T., Li, X.D., Chen, X., Li, Q.Z., Wight-Carter, M., and Chen, Z.J. (2015). Activation of
1142 cyclic GMP-AMP synthase by self-DNA causes autoimmune diseases. *Proc Nat Acad Sci*
1143 *USA 112*, E5699-5705.
1144 Gao, P., Ascano, M., Wu, Y., Barchet, W., Gaffney, B.L., Zillinger, T., Serganov, A.A., Liu, Y.,
1145 Jones, R.A., Hartmann, G.*, et al.* (2013a). Cyclic [G(2',5')pA(3',5')p] is the metazoan
1146 second messenger produced by DNA-activated cyclic GMP-AMP synthase. *Cell 153*,
1147 1094-1107.
1148 Gao, P., Ascano, M., Zillinger, T., Wang, W., Dai, P., Serganov, A.A., Gaffney, B.L., Shuman, S.,
1149 Jones, R.A., Deng, L.*, et al.* (2013b). Structure-function analysis of STING activation by
1150 c[G(2',5')pA(3',5')p] and targeting by antiviral DMXAA. *Cell 154*, 748-762.
1151 Garcia-Martinez, I., Santoro, N., Chen, Y., Hoque, R., Ouyang, X., Caprio, S., Shlomchik, M.J.,
1152 Coffman, R.L., Candia, A., and Mehal, W.Z. (2016). Hepatocyte mitochondrial DNA drives
1153 nonalcoholic steatohepatitis by activation of TLR9. *J Clin Invest 126*, 859-864.
1154 Hanada, K., Uchida, T., Tsukamoto, Y., Watada, M., Yamaguchi, N., Yamamoto, K., Shiota, S.,
1155 Moriyama, M., Graham, D.Y., and Yamaoka, Y. (2014). *Helicobacter pylori* infection
1156 introduces DNA double-strand breaks in host cells. *Infect Immun 82*, 4182-4189.
1157 Ishii, K.J., Coban, C., Kato, H., Takahashi, K., Torii, Y., Takeshita, F., Ludwig, H., Sutter, G.,
1158 Suzuki, K., Hemmi, H.*, et al.* (2006). A Toll-like receptor-independent antiviral response
1159 induced by double-stranded B-form DNA. *Nat Immunol 7*, 40-48.
1160 Ishikawa, H., and Barber, G.N. (2008). STING is an endoplasmic reticulum adaptor that facilitates
1161 innate immune signalling. *Nature 455*, 674-678.

1162 Ishikawa, H., Ma, Z., and Barber, G.N. (2009). STING regulates intracellular DNA-mediated, type
1163 I interferon-dependent innate immunity. *Nature 461*, 788-792.
1164 Johnson, E.M., Gaddy, J.A., Voss, B.J., Hennig, E.E., and Cover, T.L. (2014). Genes required for
1165 assembly of pili associated with the *Helicobacter pylori cag* type IV secretion system.
1166 *Infect Immun 82*, 3457-70.
1167 Ke, X., Hu, T., and Jiang, M. (2022). cGAS-STING signaling pathway in gastrointestinal
1168 inflammatory disease and cancers. *FASEB J 36*, e22029.
1169 Kidane, D. (2018). Molecular mechanisms of *H. pylori*-Induced DNA double-strand breaks. *Int J*
1170 *Mol Sci 19*.
1171 Koeppel, M., Garcia-Alcalde, F., Glowinski, F., Schlaermann, P., and Meyer, T.F. (2015).
1172 *Helicobacter pylori* infection causes characteristic DNA damage patterns in human cells.
1173 *Cell Rep 11*, 1703-1713.
1174 Ku, J.W.K., Chen, Y., Lim, B.J.W., Gasser, S., Crasta, K.C., and Gan, Y.H. (2020). Bacterial-
1175 induced cell fusion is a danger signal triggering cGAS-STING pathway via micronuclei
1176 formation. *Proc Nat Acad Sci USA 117*, 15923-15934.
1177 Kumar Pachathundikandi, S., Brandt, S., Madassery, J., and Backert, S. (2011). Induction of TLR-
1178 2 and TLR-5 expression by *Helicobacter pylori* switches *cag*PAI-dependent signalling
1179 leading to the secretion of IL-8 and TNF-alpha. *PLoS One 6*, e19614.
1180 Kuriakose, T., Man, S.M., Malireddi, R.K., Karki, R., Kesavardhana, S., Place, D.E., Neale, G.,
1181 Vogel, P., and Kanneganti, T.D. (2016). ZBP1/DAI is an innate sensor of influenza virus
1182 triggering the NLRP3 inflammasome and programmed cell death pathways. *Sci Immunol*
1183 *1*.
1184 Marinho, F.V., Benmerzoug, S., Oliveira, S.C., Ryffel, B., and Quesniaux, V.F.J. (2017). The
1185 emerging roles of STING in bacterial infections. *Trend Microbiol 25*, 906-918.
1186 McArthur, K., Whitehead, L.W., Heddleston, J.M., Li, L., Padman, B.S., Oorschot, V., Geoghegan,
1187 N.D., Chappaz, S., Davidson, S., San Chin, H.*, et al.* (2018). BAK/BAX macropores
1188 facilitate mitochondrial herniation and mtDNA efflux during apoptosis. *Science 359*.
1189 Miao, L., Qi, J., Zhao, Q., Wu, Q.N., Wei, D.L., Wei, X.L., Liu, J., Chen, J., Zeng, Z.L., Ju, H.Q.*,*
1190 *et al.* (2020). Targeting the STING pathway in tumor-associated macrophages regulates
1191 innate immune sensing of gastric cancer cells. *Theranostics 10*, 498-515.
1192 Nandakumar, R., Tschismarov, R., Meissner, F., Prabakaran, T., Krissanaprasit, A., Farahani, E.,
1193 Zhang, B.C., Assil, S., Martin, A., Bertrams, W.*, et al.* (2019). Intracellular bacteria engage
1194 a STING-TBK1-MVB12b pathway to enable paracrine cGAS-STING signalling. *Nat*
1195 *Microbiol 4*, 701-713.
1196 Oka, T., Hikoso, S., Yamaguchi, O., Taneike, M., Takeda, T., Tamai, T., Oyabu, J., Murakawa,
1197 T., Nakayama, H., Nishida, K.*, et al.* (2012). Mitochondrial DNA that sscapes from
1198 autophagy causes inflammation and heart failure. *Nature 485*, 251-255.
1199 Onomoto, K., Onoguchi, K., and Yoneyama, M. (2021). Regulation of RIG-I-like receptor-
1200 mediated signaling: interaction between host and viral factors. *Cell Mol Immunol 18*, 539-
1201 555.
1202 Peignier, A., and Parker, D. (2021). Impact of type I interferons on susceptibility to bacterial
1203 pathogens. *Trend Microbiol 29*, 823-835.
1204 Qiao, Y., Zhu, S., Deng, S., Zou, S.S., Gao, B., Zang, G., Wu, J., Jiang, Y., Liu, Y.J., and Chen,
1205 J. (2020). Human cancer cells sense cytosolic nucleic acids through the RIG-I-MAVS
1206 pathway and cGAS-STING pathway. *Front Cell Dev Biol 8*, 606001.
1207 Rad, R., Ballhorn, W., Voland, P., Eisenacher, K., Mages, J., Rad, L., Ferstl, R., Lang, R., Wagner,
1208 H., Schmid, R.M.*, et al.* (2009). Extracellular and intracellular pattern recognition receptors
1209 cooperate in the recognition of *Helicobacter pylori*. *Gastroenterology 136*, 2247-2257.
1210 Rathinam, V.A., Jiang, Z., Waggoner, S.N., Sharma, S., Cole, L.E., Waggoner, L., Vanaja, S.K.,
1211 Monks, B.G., Ganesan, S., Latz, E.*, et al.* (2010). The AIM2 inflammasome is essential
1212 for host defense against cytosolic bacteria and DNA viruses. *Nat Immunol 11*, 395-402.

1213 Rongvaux, A., Jackson, R., Harman, C.C., Li, T., West, A.P., de Zoete, M.R., Wu, Y., Yordy, B.,
1214 Lakhani, S.A., Kuan, C.Y., *et al.* (2014). Apoptotic caspases prevent the induction of type
1215 I interferons by mitochondrial DNA. *Cell 159*, 1563-1577.
1216 Salama, N.R., Hartung, M.L., and Muller, A. (2013). Life in the human stomach: persistence
1217 strategies of the bacterial pathogen *Helicobacter pylori*. *Nat Rev Microbiol 11*, 385-399.
1218 Schwartz, S.L., Park, E.N., Vachon, V.K., Danzy, S., Lowen, A.C., and Conn, G.L. (2020). Human
1219 OAS1 activation is highly dependent on both RNA sequence and context of activating
1220 RNA motifs. *Nucleic Acids Res 48*, 7520-7531.
1221 Shaffer, C.L., Gaddy, J.A., Loh, J.T., Johnson, E.M., Hill, S., Hennig, E.E., McClain, M.S.,
1222 McDonald, W.H., and Cover, T.L. (2011). *Helicobacter pylori* exploits a unique repertoire
1223 of type IV secretion system components for pilus assembly at the bacteria-host cell
1224 interface. *PLoS Pathog 7*, e1002237.
1225 Song, S., Peng, P., Tang, Z., Zhao, J., Wu, W., Li, H., Shao, M., Li, L., Yang, C., Duan, F., *et al.*
1226 (2017). Decreased expression of STING predicts poor prognosis in patients with gastric
1227 cancer. *Sci Rep 7*, 39858.
1228 Stein, S.C., Faber, E., Bats, S.H., Murillo, T., Speidel, Y., Coombs, N., and Josenhans, C. (2017).
1229 *Helicobacter pylori* modulates host cell responses by cagT4SS-dependent translocation
1230 of an intermediate metabolite of LPS inner core heptose biosynthesis. *PLoS Pathog 13*,
1231 e1006514.
1232 Stetson, D.B., and Medzhitov, R. (2006). Recognition of cytosolic DNA activates an IRF3-
1233 dependent innate immune response. *Immunity 24*, 93-103.
1234 Storek, K.M., Gertsvolf, N.A., Ohlson, M.B., and Monack, D.M. (2015). cGAS and Ifi204 cooperate
1235 to produce type I IFNs in response to *Francisella* infection. *J Immunol 194*, 3236-3245.
1236 Sun, L., Wu, J., Du, F., Chen, X., and Chen, Z.J. (2013). Cyclic GMP-AMP synthase is a cytosolic
1237 DNA sensor that activates the type I interferon pathway. *Science 339*, 786-791.
1238 Sun, W., Li, Y., Chen, L., Chen, H., You, F., Zhou, X., Zhou, Y., Zhai, Z., Chen, D., and Jiang, Z.
1239 (2009). ERIS, an endoplasmic reticulum IFN stimulator, activates innate immune signaling
1240 through dimerization. *Proc Nat Acad Sci USA 106*, 8653-8658.
1241 Sung, H., Ferlay, J., Siegel, R.L., Laversanne, M., Soerjomataram, I., Jemal, A., and Bray, F.
1242 (2021). Global Cancer Statistics 2020: GLOBOCAN estimates of incidence and mortality
1243 worldwide for 36 cancers in 185 countries. *CA Cancer J Clin 71*, 209-249.
1244 Unterholzner, L., Keating, S.E., Baran, M., Horan, K.A., Jensen, S.B., Sharma, S., Sirois, C.M.,
1245 Jin, T., Latz, E., Xiao, T.S., *et al.* (2010). IFI16 is an innate immune sensor for intracellular
1246 DNA. *Nat Immunol 11*, 997-1004.
1247 Varga, M.G., Piazuelo, M.B., Romero-Gallo, J., Delgado, A.G., Suarez, G., Whitaker, M.E.,
1248 Krishna, U.S., Patel, R.V., Skaar, E.P., Wilson, K.T., *et al.* (2016a). TLR9 activation
1249 suppresses inflammation in response to *Helicobacter pylori* infection. *Am J Physiol*
1250 *Gastrointest Liver Physiol 311*, G852-G858.
1251 Varga, M.G., Shaffer, C.L., Sierra, J.C., Suarez, G., Piazuelo, M.B., Whitaker, M.E., Romero-
1252 Gallo, J., Krishna, U.S., Delgado, A., Gomez, M.A., *et al.* (2016b). Pathogenic
1253 *Helicobacter pylori* strains translocate DNA and activate TLR9 via the cancer-associated
1254 *cag* type IV secretion system. *Oncogene 35*, 6262-6269.
1255 Varga, M.G., Wood, C.R., Butt, J., Ryan, M.E., You, W.C., Pan, K., Waterboer, T., Epplein, M.,
1256 and Shaffer, C.L. (2021). Immunostimulatory membrane proteins potentiate *H. pylori*-
1257 induced carcinogenesis by enabling CagA translocation. *Gut Microbes 13*, 1-13.
1258 Viala, J., Chaput, C., Boneca, I.G., Cardona, A., Girardin, S.E., Moran, A.P., Athman, R., Memet,
1259 S., Huerre, M.R., Coyle, A.J., *et al.* (2004). Nod1 responds to peptidoglycan delivered by
1260 the *Helicobacter pylori cag* pathogenicity island. *Nat Immunol 5*, 1166-1174.
1261 Watanabe, T., Asano, N., Fichtner-Feigl, S., Gorelick, P.L., Tsuji, Y., Matsumoto, Y., Chiba, T.,
1262 Fuss, I.J., Kitani, A., and Strober, W. (2010). NOD1 contributes to mouse host defense

1263 against *Helicobacter pylori* via induction of type I IFN and activation of the ISGF3 signaling
1264 pathway. *J Clin Invest 120*, 1645-1662.
1265 Watson, R.O., Bell, S.L., MacDuff, D.A., Kimmey, J.M., Diner, E.J., Olivas, J., Vance, R.E.,
1266 Stallings, C.L., Virgin, H.W., and Cox, J.S. (2015). The cytosolic sensor cGAS detects
1267 *Mycobacterium tuberculosis* DNA to induce type I interferons and activate autophagy. *Cell*
1268 *Host Microbe 17*, 811-819.
1269 West, A.P., Khoury-Hanold, W., Staron, M., Tal, M.C., Pineda, C.M., Lang, S.M., Bestwick, M.,
1270 Duguay, B.A., Raimundo, N., MacDuff, D.A.*, et al.* (2015). Mitochondrial DNA stress
1271 primes the antiviral innate immune response. *Nature 520*, 553-557.
1272 White, M.J., McArthur, K., Metcalf, D., Lane, R.M., Cambier, J.C., Herold, M.J., van Delft, M.F.,
1273 Bedoui, S., Lessene, G., Ritchie, M.E.*, et al.* (2014). Apoptotic caspases suppress mtDNA-
1274 induced STING-mediated type I IFN production. *Cell 159*, 1549-1562.
1275 Wu, J., Sun, L., Chen, X., Du, F., Shi, H., Chen, C., and Chen, Z.J. (2013). Cyclic GMP-AMP is
1276 an endogenous second messenger in innate immune signaling by cytosolic DNA. *Science*
1277 *339*, 826-830.
1278 Wu, X.M., Zhang, J., Li, P.W., Hu, Y.W., Cao, L., Ouyang, S., Bi, Y.H., Nie, P., and Chang, M.X.
1279 (2020). NOD1 promotes antiviral signaling by binding viral RNA and regulating the
1280 interaction of MDA5 and MAVS. *J Immunol 204*, 2216-2231.
1281 Zhang, Q., Raoof, M., Chen, Y., Sumi, Y., Sursal, T., Junger, W., Brohi, K., Itagaki, K., and
1282 Hauser, C.J. (2010). Circulating mitochondrial DAMPs cause inflammatory responses to
1283 injury. *Nature 464*, 104-107.
1284 Zhang, X., Bogunovic, D., Payelle-Brogard, B., Francois-Newton, V., Speer, S.D., Yuan, C., Volpi,
1285 S., Li, Z., Sanal, O., Mansouri, D.*, et al.* (2015). Human intracellular ISG15 prevents
1286 interferon-alpha/beta over-amplification and auto-inflammation. *Nature 517*, 89-93.
1287 Zhang, X., Shi, H., Wu, J., Zhang, X., Sun, L., Chen, C., and Chen, Z.J. (2013). Cyclic GMP-AMP
1288 containing mixed phosphodiester linkages is an endogenous high-affinity ligand for
1289 STING. *Mol Cell 51*, 226-235.
1290 Zhang, Y., Yeruva, L., Marinov, A., Prantner, D., Wyrick, P.B., Lupashin, V., and Nagarajan, U.M.
1291 (2014). The DNA sensor, cyclic GMP-AMP synthase, is essential for induction of IFN-beta
1292 during *Chlamydia trachomatis* infection. *J Immunol 193*, 2394-2404.
1293 Zhong, B., Yang, Y., Li, S., Wang, Y.Y., Li, Y., Diao, F., Lei, C., He, X., Zhang, L., Tien, P.*, et al.*
1294 (2008). The adaptor protein MITA links virus-sensing receptors to IRF3 transcription factor
1295 activation. *Immunity 29*, 538-550.
1296 Zimmermann, S., Pfannkuch, L., Al-Zeer, M.A., Bartfeld, S., Koch, M., Liu, J., Rechner, C.,
1297 Soerensen, M., Sokolova, O., Zamyatina, A.*, et al.* (2017). ALPK1- and TIFA-dependent
1298 innate immune response triggered by the *Helicobacter pylori* type IV secretion system.
1299 *Cell Rep 20*, 2384-2395.
1300

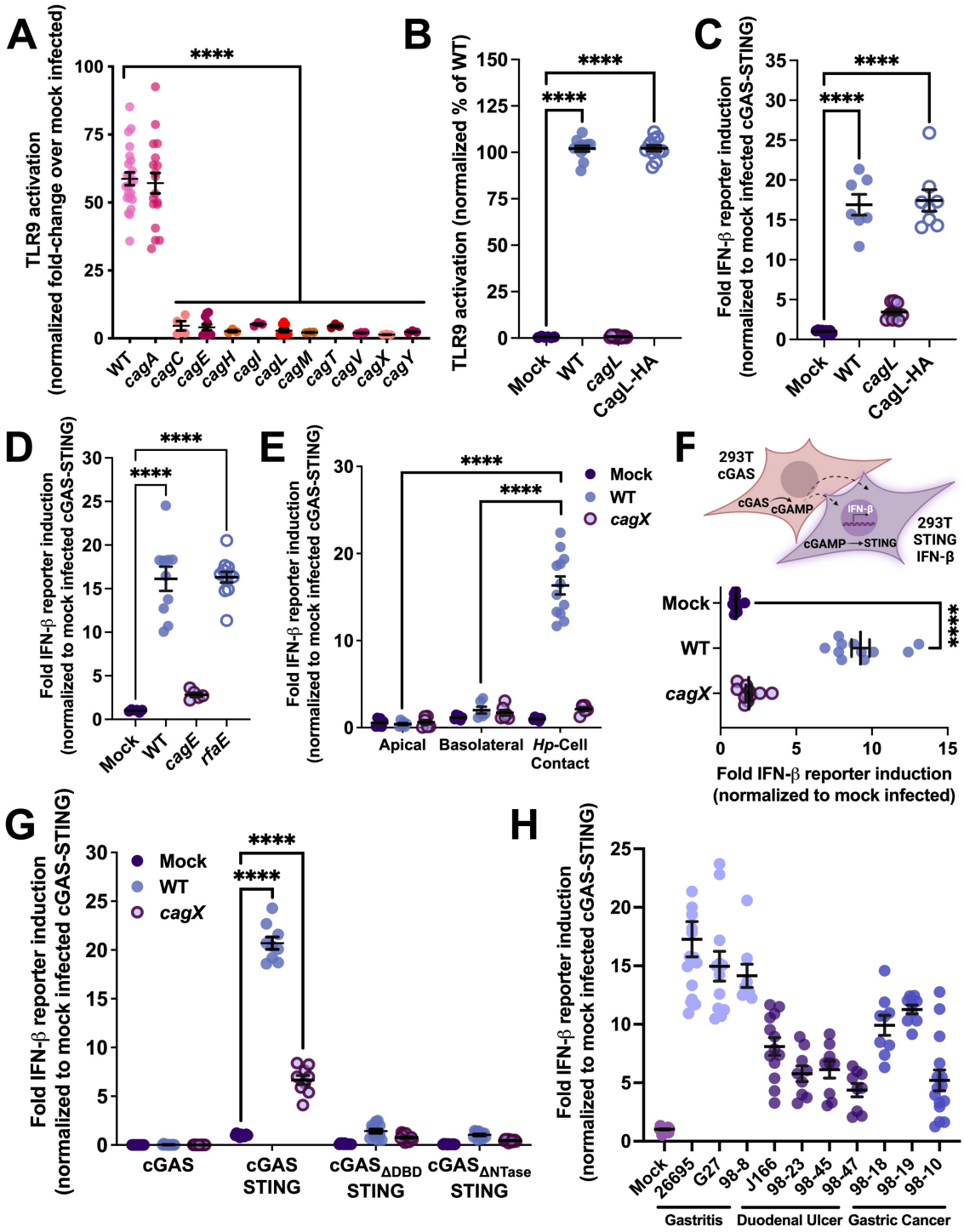

Figure 1. *H. pylori cag* T4SS activity stimulates multiple DNA surveillance systems. A. TLR9 activation induced by the indicated *H. pylori* 26695 isogenic mutant strain. Data are expressed as the normalized fold change over mock infected cells. **B**. TLR9 activation requires a functional *cag* T4SS. **C**. cGAS-STING signaling stimulated by the indicated strain. **D**. Induction of double-stranded DNA breaks in the host genome does not significantly contribute to *H. pylori*-induced

cGAS-STING signaling. Graph depicts IFN-β reporter activity induced in cGAS-STING reporter cells by the indicated strain. **E**. Transwell cGAS-STING activation assays demonstrating the requirement for direct bacteria-host cell contact. **F**. STING transactivation assays providing evidence of intercellular cGAMP transfer. Schematic depicts the reporter cell line experimental strategy. **G**. IFN-β transcriptional reporter assays demonstrating the requirement of the cGAS DNA-binding domain ($cGAS_{\Delta DBD}$) and cGAS catalytic activity ($cGAS_{\Delta NTase}$) for *H. pylori*-induced cGAS-STING signaling. **H.** cGAS-STING signaling induced by the indicated *H. pylori* strain stratified by disease state (gastritis, duodenal ulcer, and gastric adenocarcinoma). In **A**-**G**, significance was determined by one-way ANOVA with Dunnett's post-hoc correction for multiple comparisons to experimental controls. In all panels, ****, $p<0.0001$.

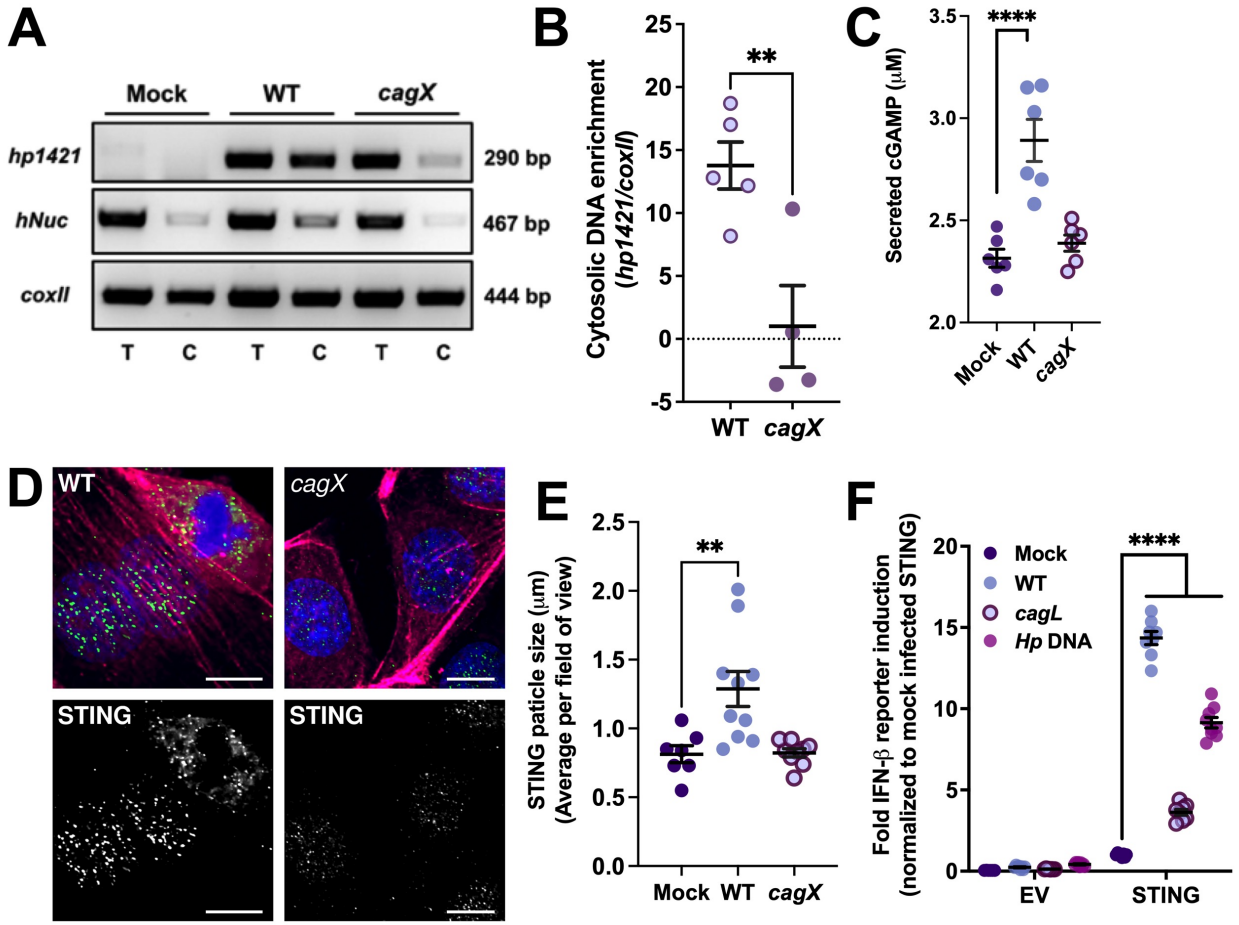

Figure 2. *H. pylori* DNA is delivered to the gastric epithelial cell cytoplasm in a *cag* T4SS-dependent manner. A. Representative PCR amplifications demonstrating the presence of chromosomal *H. pylori* (*hp1421*), nuclear genomic (*hNuc* (Fernandez-Moreno et al., 2016)), and mitochondrial (*coxII* (Fernandez-Moreno et al., 2016)) DNA fragments in fractionated cytoplasmic (C) and total (T) co-culture AGS cell extracts. **B**. qPCR analysis of *H. pylori* DNA enrichment in cytosolic fractions normalized to levels of cytosolic mitochondrial DNA. Results are representative of at least 4 biological replicate experiments. Significance was determined by unpaired, two-tailed t-test; **, $p<0.01$. **C**. Levels of extracellular cGAMP produced by AGS cells in response to *H. pylori*. **D**. Confocal microscopy analysis of perinuclear STING localization in *H. pylori*-challenged primary gastric epithelial cells at 6 h post-infection. Representative image of $n=2$ biological replicate experiments depicting STING (green), nuclei (blue), and actin (magenta) staining. Scale bar represents 20 μm. **E**. Quantitation of STING particle size in primary gastric epithelial cells challenged by the indicated *H. pylori* strain. Data represents the average STING particle size per field of view for mock infected (7 fields of view, $n=90$ cells); WT infected (11 fields of view, $n=82$ cells); and *cagX* infected (9 fields of view, $n=59$ cells) gastric epithelial cells. **F**. STING signaling induced by the indicated *H. pylori* strain or purified *H. pylori* chromosomal DNA in 293T reporter cells. Data is representative of a minimum of 3 biological replicate experiments. In **E-F**, significance was determined by one-way ANOVA with Dunnett's post-hoc correction for multiple comparisons to experimental controls; ****, $p<0.0001$.

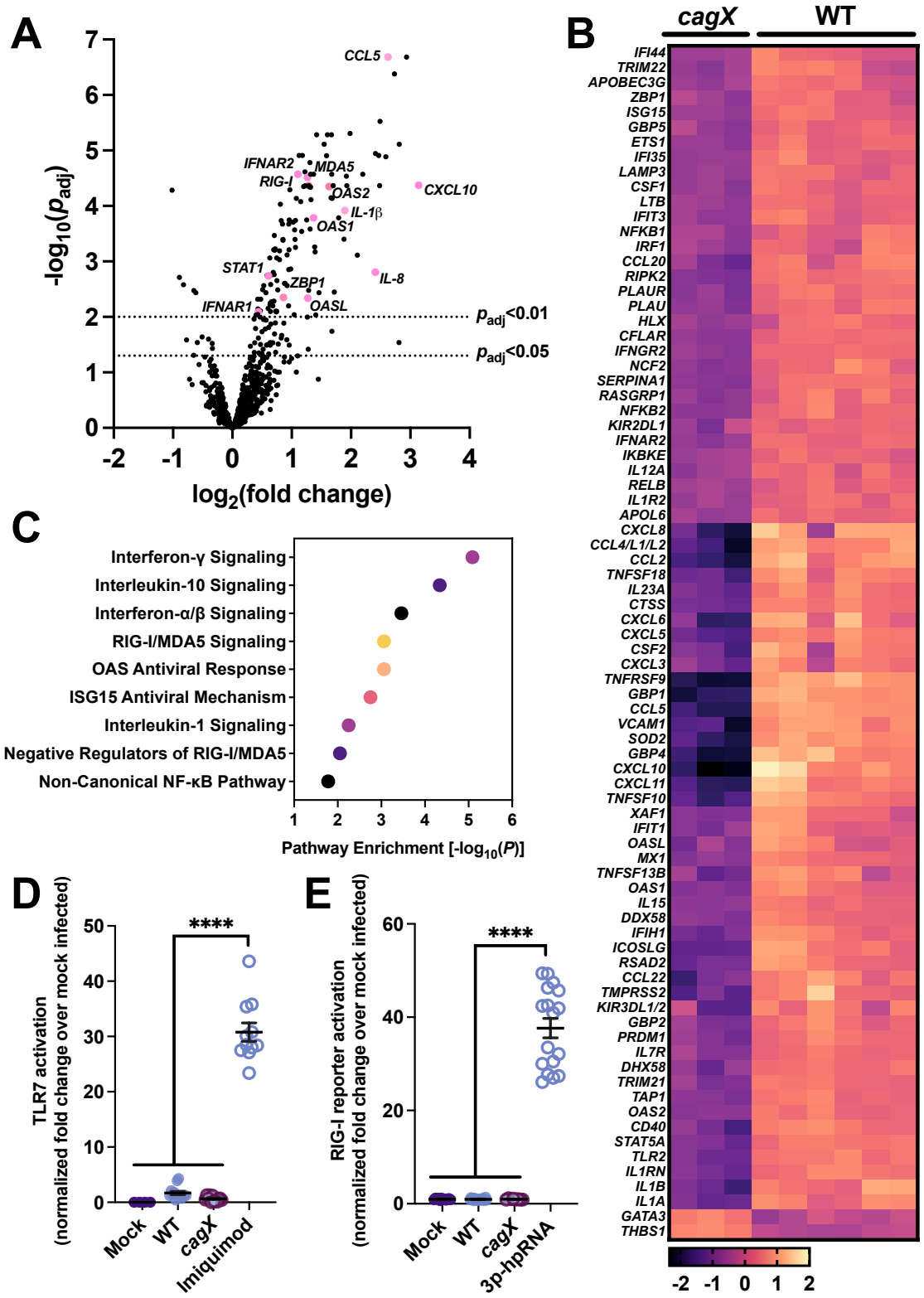

Figure 3. *H. pylori* regulates nucleic acid reconnaissance pathways via *cag* T4SS activity. **A.** Volcano plot depicting expression of immune-related genes in adult human primary epithelial cells challenged by *H. pylori* detected with the NanoString human host response panel. Graph

represents the fold change and associated *p*-value of all differentially expressed genes in the panel for WT vs. *cagX* challenged cells. Dashed lines dashed lines demarcate genes meeting the threshold for significance (p_{adj}<0.01 and p_{adj}<0.05) after correction with the Benjamini–Hochberg procedure for controlling FDR. Selected genes encoding nucleic acid sensing pathways, interferon-responsive elements, and inflammatory cytokines/chemokines are labeled and indicated in pink. **B**. Heat map of differentially expressed genes depicted in a. Map depicts genes that were increased or decreased by 1.8-fold and an adjusted *p*-value <0.01. **C**. Pathway analysis of differentially expressed immune genes. Graph depicts the -$\log_{10}$ *p*-value for the indicated pathway. **D**. TLR7 activation levels induced by the indicated strain or pharmacological stimulus. **E**. Levels of RIG-I signaling stimulated by *H. pylori* or transfected RNA agonist. In **D** and **E**, significance was determined by one-way ANOVA with Dunnett's post-hoc correction for multiple comparisons to experimental controls; ****, *p*<0.0001. Data is derived from *n*=1 NanoString analysis with gastric epithelial cell samples derived from *n*=2 biological replicate experiments (mock infected, *n*=3, WT infected *n*=6, and *cagX* infected *n*=3 samples analyzed).

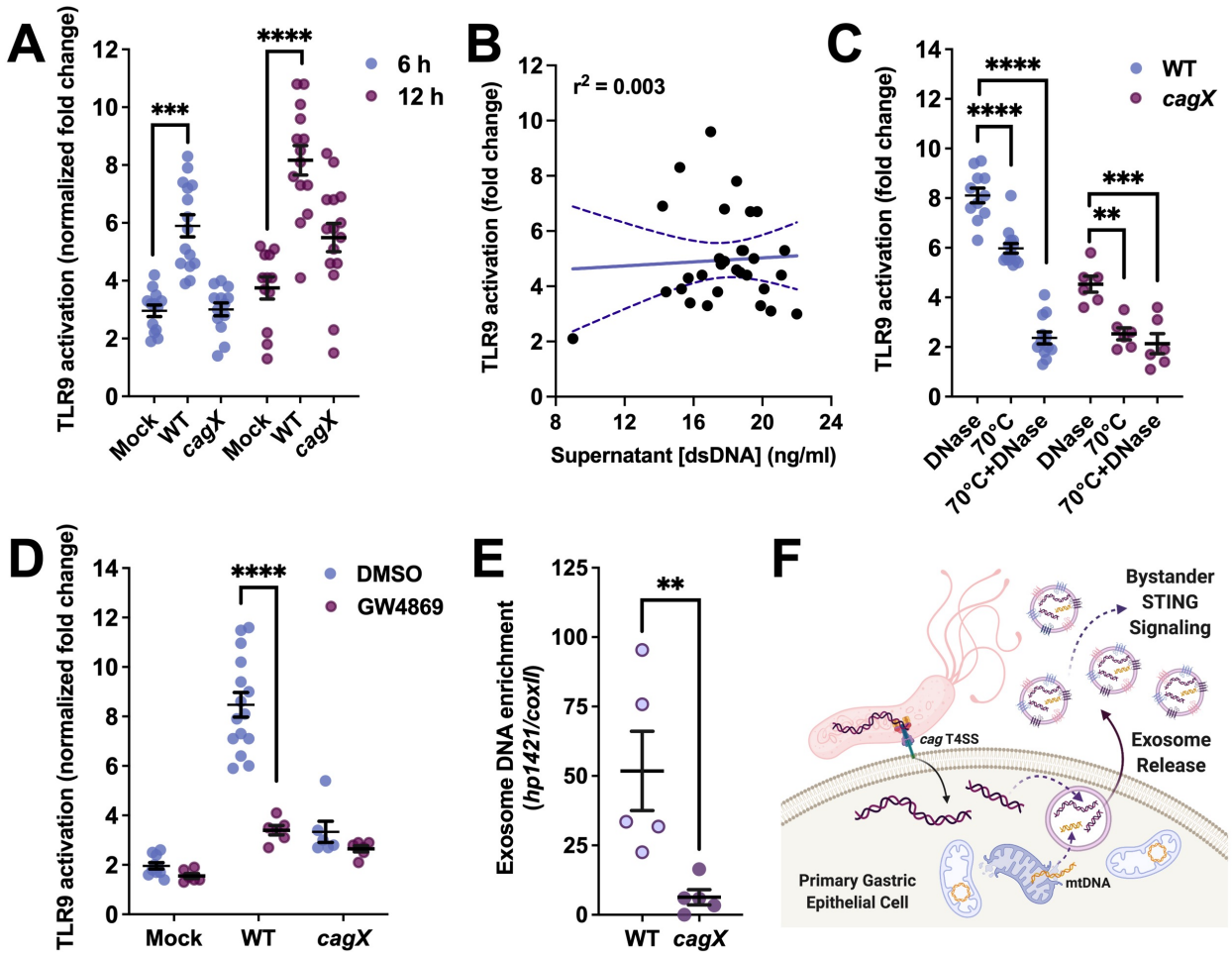

Figure 4. *H. pylori* effector DNA is packaged into exosomes to enable DNA pattern recognition receptor signaling in bystander cells. A. TLR9 stimulation induced by supernatants obtained from primary gastric epithelial cells challenged by *H. pylori* at the indicated time point post-infection. Graph depicts levels of TLR9 activation achieved by supernatants collected in a minimum of four biological replicate experiments. **B**. Linear regression analysis revealing no correlation between levels of TLR9 activation induced by gastric epithelial cell supernatants and the corresponding level of supernatant total cell-free DNA. **C**. Levels of TLR9 activation achieved by gastric cell supernatants obtained at 6 h post-infection and processed by the indicated conditions. **D**. Induction of TLR9 stimulation by gastric cell supernatant extracellular vesicles in gastric epithelial cell supernatants challenged by *H. pylori* in the presence or absence of GW4869 (10 μM). Significance was determined by unpaired, two-tailed t-test; ****, $p<0.0001$. **E**. qPCR analysis of *H. pylori* DNA enrichment in purified exosomes derived from primary gastric epithelial co-culture supernatants 6 h post-bacterial challenge by the indicated strain. Graph depicts the fold enrichment of *H. pylori* DNA (*hp1421*) over levels of mitochondrial DNA (*coxII*) in exosomes purified from supernatants collected from five biological replicate experiments. Significance was determined by unpaired, two-tailed t-test; **, $p<0.01$. **F**. Schematic representing a proposed model of translocated *H. pylori* DNA packaging and subsequent release of extracellular vesicles by primary gastric cells. In **A** and **C**, significance was determined by one-way ANOVA with Dunnett's post-hoc correction for multiple comparisons to experimental controls; ****, $p<0.0001$, ***, $p<0.001$, and **, $p<0.01$.

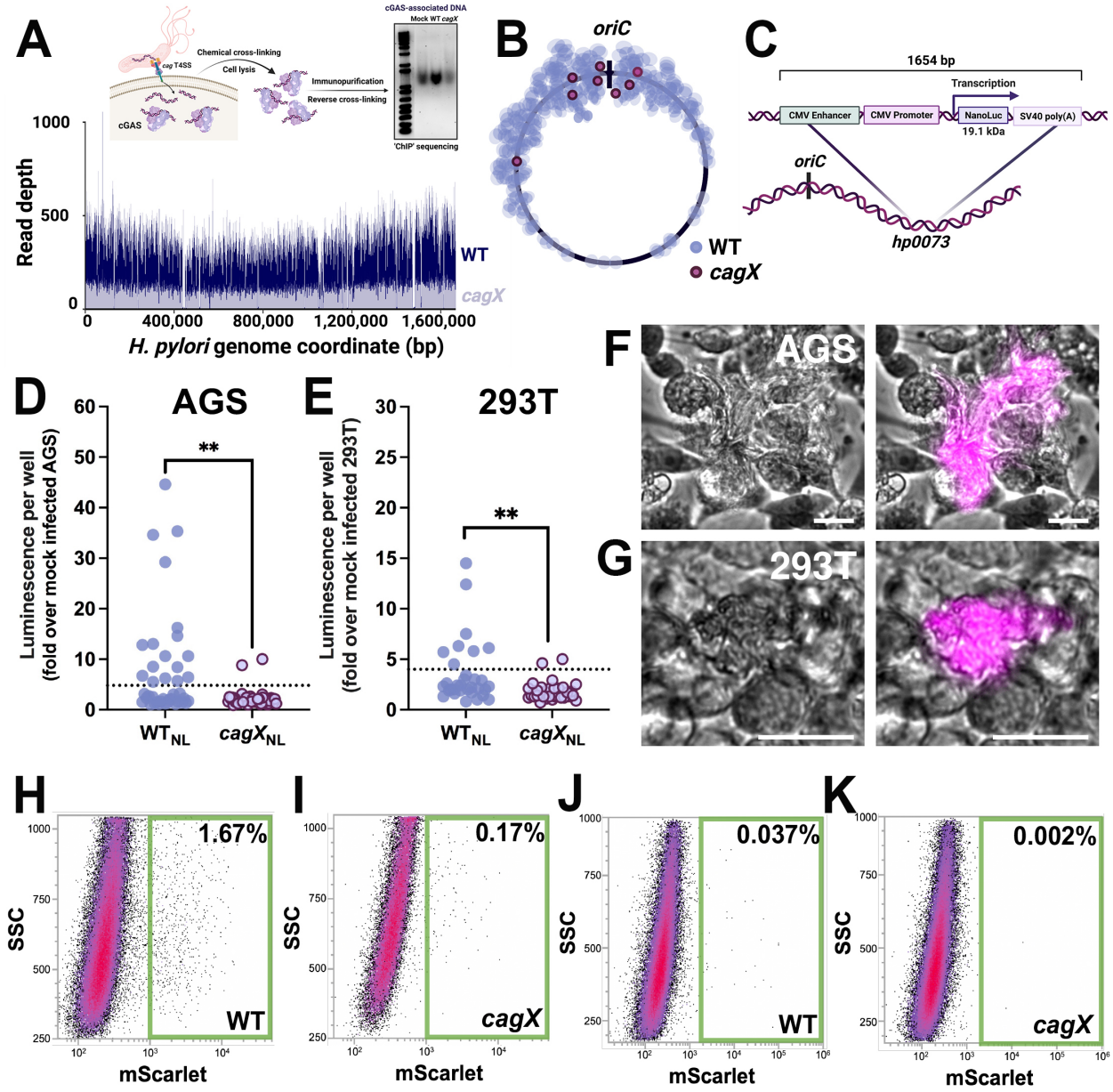

Figure 5. Chromosomally-derived DNA is translocated into target cells via *cag* T4SS mechanisms. A. Merged tracks of mapped *H. pylori* DNA reads obtained from infected 293T cGAS cells. Graph depicts sequencing read depth versus nucleotide position in the *H. pylori* 26695 genome. Schematic illustrates the experimental workflow for cGAS 'ChIP-seq' studies. **B**. DNA reads co-purified with cGAS were normalized to reads obtained from mock infected cells, and peak calling was used to identify regions of bacterial DNA that were enriched with cGAS immunopurification. Dots depict individual peaks and the corresponding peak center on the *H. pylori* 26695 chromosome obtained from WT (purple dots) and *cagX* (maroon dots) challenged co-cultures. **C**. Schematic of eukaryotic-optimized nanoluciferase expression constructs inserted into the *hp0073* locus. Nanoluciferase constructs were inserted frameshifted in the opposite orientation of the native operon transcription. **D**,**E**. Nanoluciferase bioluminescence produced by

AGS (**D**) and 293T (**E**) cells challenged by the indicated strain at 24 h post-infection. Data represent a minimum of four biological replicate experiments. Significance was determined by unpaired, two-tailed t-test; **, $p<0.01$. **F,G**. Live cell, phase contrast and fluorescence microscopy analysis of AGS (**F**) and 293T (**G**) cells challenged by WT *H. pylori* harboring LifeAct-mScarlet expression constructs at 24 h post-infection. Images are representative of $n=2$ biological replicate experiments. **H-K**. Flow cytometry analysis of AGS (**H** and **I**) or 293T cells (**J** and **K**) challenged by WT[mScarlet] or *cagX*[mScarlet] at 18 h post-infection. Green boxes indicate gating of mScarlet positive cells. Data is representative of $n=2$ biological replicate experiments.

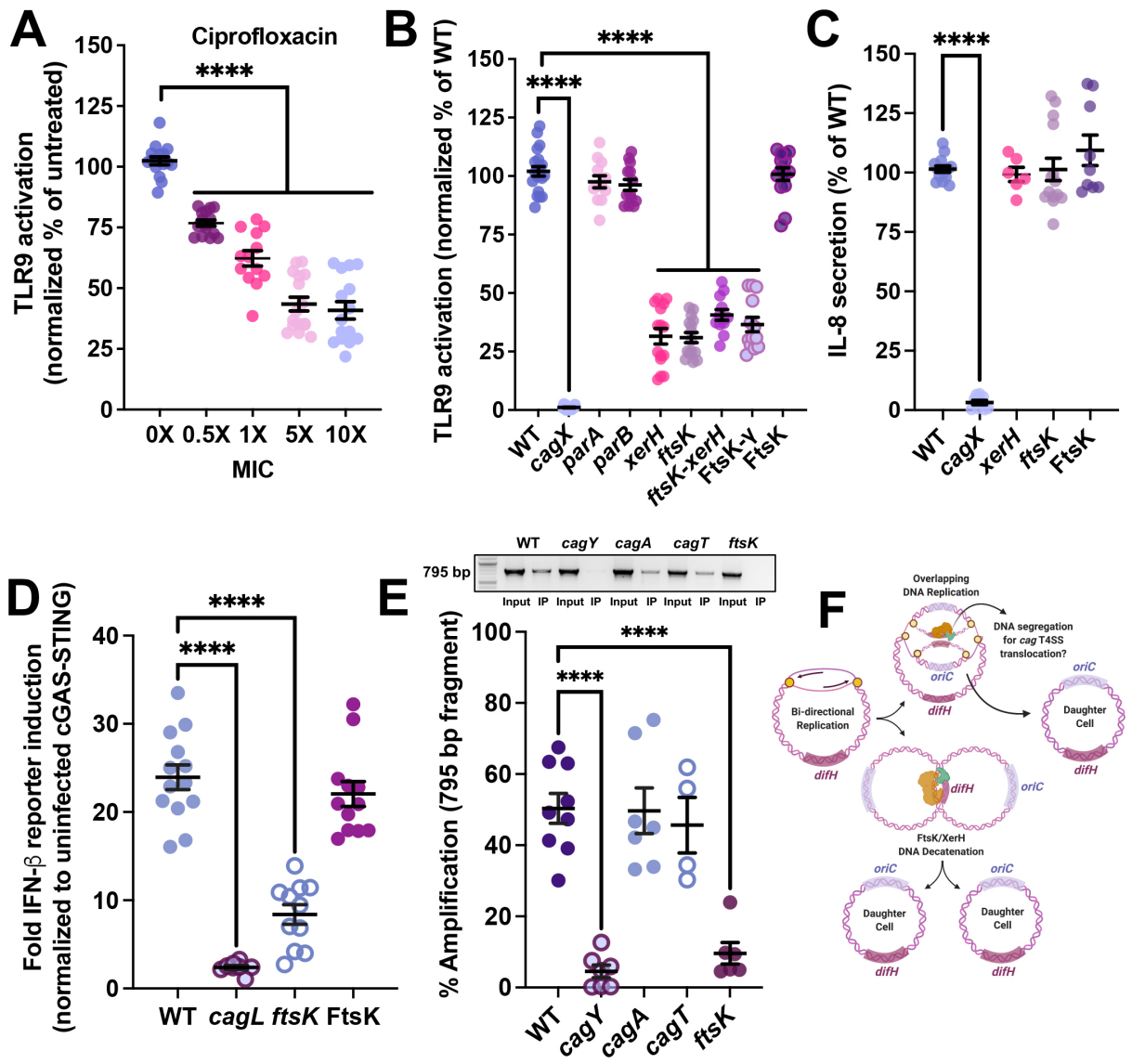

Figure 6. DNA translocation is mechanistically coupled to chromosomal replication and replichore decatenation. A. TLR9 activation induced by WT *H. pylori* in the presence of the indicated ciprofloxacin minimum inhibitory concentration (1X MIC = 0.125 µg/ml). Data are expressed as a percent of TLR9 stimulation achieved by WT in mock treated wells. **B**. Levels of TLR9 activation induced by the indicated isogenic mutant. Data are expressed as a percent of TLR9 stimulation achieved by the parental WT strain. **C**. IL-8 secreted by AGS cells challenged by the indicated *H. pylori* strain at 4.5 h post-infection. Data are expressed as a percent of IL-8 levels stimulated by the corresponding WT strain. **D**. cGAS-STING signaling induced by the indicted strain. Graph depicts the results of *n*=3 biological replicate experiments. **E**. Transfer DNA immunopurification assays demonstrating the presence of *H. pylori* chromosomal DNA fragments within the *cag* T4SS apparatus. Graph depicts the amplification efficiency of a 795 bp fragment in transfer DNA assay preparations purified from the indicated strain. Amplification efficiency of the immunopurification (IP) samples are expressed as the percent of the input DNA from at least four biological replicate experiments. Inset depicts representative PCR amplifications obtained from

input and IP samples prepared from the indicated strain. **F**. Proposed model of DNA cargo segregation for *cag* T4SS-dependent delivery to host cells. We hypothesize that FtsK-XerH complexes mediate the rare excision of DNA arising from overlapping rounds of chromosomal replication for subsequent coupling to the *cag* T4SS apparatus for delivery to host cells. In **A**-**E**, significance was determined by one-way ANOVA with Dunnett's post-hoc correction for multiple comparisons to experimental controls; ****, $p<0.0001$ in all panels.